University of Padova

UNIVERSITY OF PADOVA

—

Department Of Information Engineering

—

Master thesis in Telecommunication Engineering

DEVELOPMENT OF A FIBRE OPTIC DISTRIBUTED ACOUSTIC SENSOR

Advisor: Prof. Luca Palmieri

Student: **ENRICO TOIGO**

Academic Year 2015/2016

Alla mia famiglia e ai miei nonni

Acknowledgements

Desidero ringraziare tutte le persone che mi hanno sostenuto in questo periodo di tesi con i loro consigli e le giuste parole, anche quando ogni speranza sembrava perduta. Tra tutti ringrazio soprattutto il prezioso amico Marco (con il quale non ci si annoia mai) sia per le varie e indimenticabili avventure vissute assieme, ma anche perché, con le sue sincere opinioni, mi permette di vedere le cose da un'altra prospettiva. Ringrazio Ibra che, oltre ad avere sempre pronta una risposta ad ogni mia domanda, ha sempre preso in "seria" considerazione ogni discorso fatto. Voglio ringraziare il mago della caccia Giorgio per avermi dato la possibilità di seguirlo durante le uscite mattutine e anche per i deliziosi prodotti di norcineria. Un grazie sincero a Mirko che è presente in ogni momento e a Nicola, Diego, Davide, Sara e Ugo.

Abstract

Fibre optic Distributed Acoustic Sensor (DAS) is a particular sensor which offers the possibility of measuring at thousands of points simultaneously only using, as sensing mean, the normal optical fibre. With this technology is possible to sense both static and dynamic events such as time varying-signals, vibrations, crack of the bridges...
There are different techniques that can be used for obtaining data from these distributed sensors.
In this thesis the so called Φ-OTDR is treated. This method exploits the Rayleigh backscattered power and a highly coherent laser. In addition to that an implementation of this distributed sensing system is also presented, which has been tested with three different sensor realizations. The detected traces are successively analysed in order to localize, in the frequency domain, the acoustic wave perturbations.

Contents

List of Figures

LIST OF FIGURES

LIST OF FIGURES

List of Tables

LIST OF TABLES

1

Introduction

Fibre optics sensing is a constant improvement field, both for the peculiarity of the sensing mean and for the variety of application areas. Using the fibre as a sensing element offer many advantages which are not presented with respect to other sensing systems - electrical and mechanical ones. Such advantages given by the fibre are principally: cheapness, lightly intrusive mean, high sensitivity, high level of integrability, multiplexing property, corrosion resistance and last but not least the immunity to the electromagnetic interferences.
Optical fibre offers a wide variety of properties which make it one of the best choice for monitoring big structures as buildings, bridges, dams, oil reservoirs...
An interesting key point of the physical properties of optical fibre is its high melting point which makes the fibre very useful while used for sensing activities in harsh environments.
In addition to that, the transmitted signal along the fibre, is sensitive to the surrounded environment. This make possible to measure acoustic waves (vibrations), strains, temperature, electromagnetic fields.
In the past a particular kind of sensor based on Bragg gratings integrated into the fibre has been studied. It is also known as quasi distributed sensor. This par-

ticular sensor is very cheap to create and can provide a finite number of sensitive points to the surrounding environment parameters. Another advantage of this technology is the great integrability with the structure under observation with respect to other kind of sensing systems which need unwieldy support structures. This technology suffers of some important disadvantages such as the great quantity of Bragg gratings to be created into the fibre to monitor even a small area of interest, in addition to the fact that, if a particular event happens in an area between two sensing points, this event will not be recorded. This technology is not suitable for spatial distributed measurements over long distances.
In some situations is required to have a spatial continuous measure in order to capture any kind of events along the area under observation. These sensors, with this important characteristic, are called distributed optical fibre sensors or also DOFS.
The two different sensing configurations (quasi-distributed and distributed) are presented in figure (1.1).

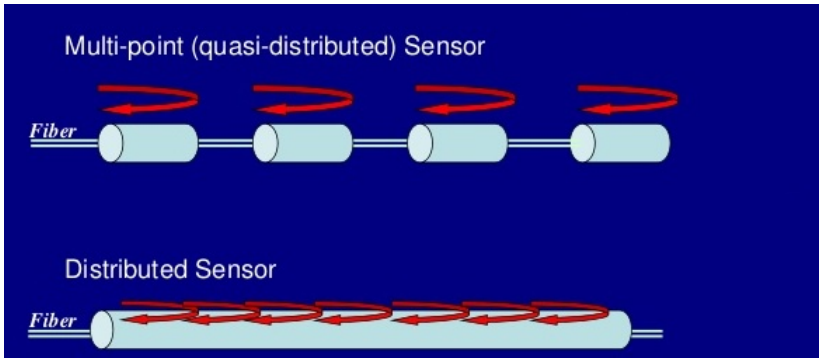

Figure 1.1: Quasi-distributed and distributed fibre optic sensing configurations.

The monitoring and localization of the physical events can be done using the transmission of short-time and high-power pulses which travel along the fibre while a portion of the radiation is scattered due to elastic or inelastic effects that are influenced by the physical quantity [13]. One part of this scattered signal, which back propagates till the input side of the fibre, is captured and processed by the computational unit.
There are three particular kinds of scattering which are used for different scopes. The most common distributed sensing methods are based on Rayleigh scattering

[9].
The backscattered signal can be acquired by an Optical Time Domain Reflectometer (OTDR), but, for sake of clearness, there are also other techniques based on frequency domain which will not be treated in this thesis.
Speaking about the time domain, when the back scattered signal reaches the detector some information can be taken depending on which parameters are considered: attenuation, phase, polarization.
In order to measure these parameter different kinds of OTDR have been studied and developed.
This thesis will focus on a particular new kind of DOFS oriented on acoustic sensing; they are called distributed acoustic sensors (DAS) based on Rayleigh scattering. The implemented technique, in order to measure this signal, and more precisely the phase variations induced by the acoustic waves on the backscattered signal, uses the phase-sensitive OTDR or ϕ-OTDR.
The thesis is structured in the following way: in *chapter one* a brief theoretical background will be introduced in order to give the basis to the concepts which will be described in the subsequent chapters. In *chapter two* there will be a description of the experimental setups that have been implemented and the used instruments. In *chapter three* the obtained results are presented and commented.

2

Theoretical background

In this chapter a brief description of some theoretical aspects is given. It will be useful for understanding the following chapters in which the used setup and the obtained results will be described.

2.1 Rayleigh scattering

Rayleigh scattering has been previously mentioned, and it is one of the basic principles of this work. First of all one brief preface about optical fibre light propagation and interaction with the mean structure is required.
The fibre optic is a very tiny glass wire as thick as a human hair. The structure of this wire appears as a core, in the center, with a refractive index slightly greater than the outside coverage structure called cladding. Exploiting this particular structure it is possible to define a reference angle θ_c, such that the light that reflects onto the core/cladding interface with an angle larger than θ_c totally reflected inside the core.
This can be described as follow: let's consider a transmitted uniform plane wave in a separation plane between two different homogeneous means then (Snell's

law):

$$n_1 \sin\theta_i = n_2 \sin\theta_t \rightarrow \text{if } n_1 > n_2,\ \exists\, \theta_t \rightarrow \theta_i < \theta_c = \arcsin\frac{n_2}{n_1} \tag{2.1}$$

Where $n_1,\ n_2,\ \theta_i,\ \theta_t$ are respectively the refractive index of the first and second mean, the incidence angle and the refraction angle.
In order to obtain the total internal reflection while transmitting light inside the optical fibre, considering n_1 as the core refractive index and n_2 as the cladding refractive index, is necessary that $\theta_i > \theta_c$.

Exploiting this concept it is possible to transmit light confined into the core and then enclose all the light power and avoid additional losses. In this thesis a monochromatic light transmitted into a single mode fibre is considered, which ensure the light to be in a single polarization state over the fibre length. This latter aspect can be obtained working on the fibre geometry and structure related to the used wavelength in order to have a single mode propagation.
Previously the term *sensibility* has been mentioned, in fact geometry is not the only parameter which affects the propagating light but also every external phenomena as acoustic waves, temperature and pressure variations, which affect the refractive index of the fibre. Fibre sensing exploit these variations and the propagating mode to perform the interested sensing measurements.

When the light travel along the fibre, it interacts with atoms and molecules of the mean. The variations of some interested parameters in the environment in which the fibre is installed alter the atoms and molecules properties that consequently alter the propagating mode state[14].
The interaction between the light and the small particles of the matter causes a decrease of the light power because these particles absorb part of the light and retransmit it over all the directions, at the same incidence wavelength, or they release it as heat.
Now, someone could ask how is possible that an optical fibre can measure only some of the big amount of parameters that can affect the fibre properties. In order to measure only some of the influences that the fibre undergoes it is necessary to build a specific setup. In fact each setup is studied and performed specifically for the interested parameters. And it is also necessary that the receiver block

system is only sensitive to the power of the modes and not to the received mode structure.
Previously a concept, in which the incident light on the mean particles can create propagation of the light over all the directions, has been mentioned: this phenomena is called scattering. There are three different kind of scattering spectral parts - see figure (2.1) - which can be detected: Rayleigh, Brillouin and Raman[4, 8].

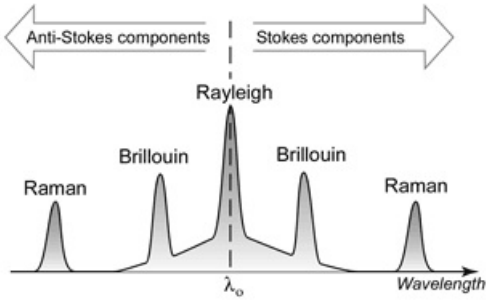

Figure 2.1: Different components of the scattering light.

The Rayleigh scattering is the dominant attenuation factor, in single mode fibres - it counts for the 96% of the total fibre loss [5]. As mentioned before the scattering spreads the light in all over the possible directions but just a small part of this light will propagate in the reverse direction - with respect to the transmitted light (see figure 2.2). Rayleigh scattering loss evolution is proportional to $\sim \frac{1}{\lambda^4}$ with increasing wavelength. This evolution has a minimum of 0.2 dB/km at $\lambda = 1550\ nm$ as shown in figure (2.3). Rayleigh phenomenon is used in OTDR to evaluate attenuations along the fibre length.

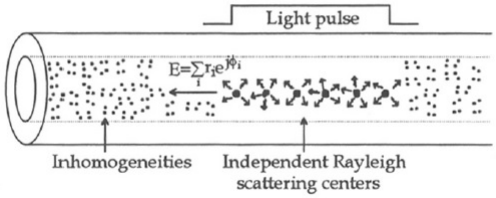

Figure 2.2: Rayleigh scattering. The variations of the refractive index has been modelled as scattering centers inside the homogeneous material, with size smaller than the optical wavelengths [6]. These scattering centers has a fixed position and they don't vary the frequency of the scattered light, with respect to the incident one. For these reasons Rayleigh scattering is also known as quasi-elastic scattering.

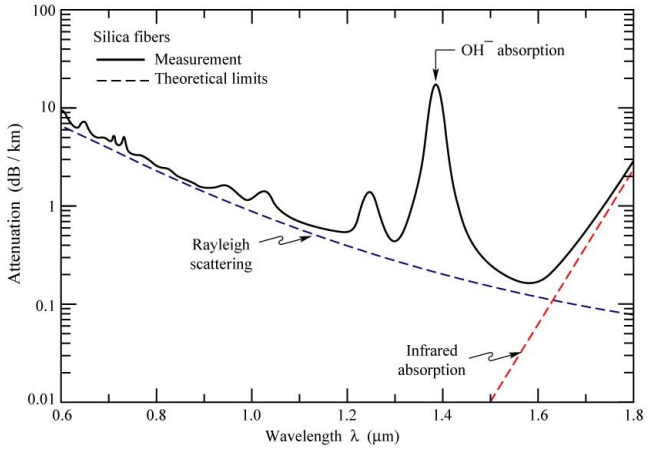

Figure 2.3: Fibre optic attenuation spectrum in which is shown Rayleigh scattering.

Let's consider the transmission of a light pulse, then the backscattering light of this transmitted rectangular pulse of width W and frequency f in a single mode-fibre can be described by the following equation:

$$e(t) = \sum_{i=1}^{N} a_i e^{-\alpha \frac{c\tau_i}{n} + j2\pi f(t-\tau_i)} rect\left(\frac{t-\tau_i}{W}\right) \tag{2.2}$$

The input light is considered monochromatic and coherent. $e(t)$ represents

the superposition of coherent light backscattered by the fibre optics small particles refractive index inhomogeneities. These particle reflects the light with the same phase and polarization of the incident light, but with different intensity. a_i represents the amplitude and $\tau_i = 2nz_i/c$ is the group delay introduced by the scattering of the ith point, N is the total number of scattering centers, α is the attenuation, c is the speed of light, n is the refractive index of the fibre, z_i is the position of the ith scattering point. The following term that accounts for the change in the scattering volume; seen as the pulse propagates, is described as:

$$rect\left[(t-\tau_i)/W\right] = \begin{cases} 1 & \text{for} \quad 0 \leq (t-\tau_i)/W \leq 1 \\ 0 & \text{otherwise} \end{cases} \tag{2.3}$$

Now let's call the received optical power with p(t), then it can be given by the following realtion [16]:

$$\begin{aligned} p(t) &= |e(t)|^2 = p_1(t) + p_2(t) \\ p_1(t) &= \sum_{i=1}^{N} a_i^2 e^{-2\alpha\frac{c\tau_i}{n}} rect\left(\frac{t-\tau_i}{W}\right) \\ p_2(t) &= 2\sum_{i=1}^{N}\sum_{j=i+1}^{N} a_i a_j \cos(\phi_{ij}) e^{-\alpha\frac{c(\tau_i+\tau_j)}{n}} rect\left(\frac{t-\tau_i}{W}\right) rect\left(\frac{t-\tau_j}{W}\right) \end{aligned} \tag{2.4}$$

where $\phi_{ij} = 2\pi f(\tau_i - \tau_j) = \frac{4\pi f n s_{ij}}{c}$ and it represents the phase difference between the scattering light transmitted by scattered points (the ith and the jth) while $s_{ij} = z_i - z_j$ is the distance between the two points. The term $p_1(t)$ represents the sum of the power scattered by N scattering points. This quantity doesn't change significantly with respect to the fibre properties or with the pulse frequency variation. The interesting term is $p_2(t)$ which is sensitive to the interferences between scattered points. This perturbations sensitivity is contained in the term ϕ. Thus $p(t)$ is a function of f, n, s_{ij}. For this reason successively will be introduced an instrument, similar to $OTDR$, but which is very sensitive to phase variations. In this thesis will be exploit the fact that varying n and s_{ij}, using an acoustic wave, is possible to determine this perturbation, analysing the phase changes. In fact when an acoustic wave propagates in a mean, it generates a deformation which varies the local density of the means and consequently the local refractive index.

2.1.1 DAS, DTS, DTSS

In figure (2.1) other different scattering with respect to Rayleigh one are depicted. Raman scattering, considering anti-Stokes components, is fibre temperature dependent while Brillouin is fibre density dependent - this makes Brillouin scattering useful for monitoring strain or temperature phenomena. Rayleigh scattering is typically used to track and to reveal propagation effects such as propagation effects, e.g. attenuation, phase interferences, polarization variations. In general these propagation effects can affect both Raman and Brillouin but they offer direct scattering sensing mechanism and thus these variations analysis are neglected [9].
There are different ways of sensing temperature, strain and acoustic waves, for example:

- *Distributed Temperature Sensors* (DTS) exploit Raman backscattering light for temperature sensing.
- *Distributed Temperature and Strain Sensing* (DTSS) uses the sensitivity of Brillouin frequency shift for temperature and strain sensing.
- *Distributed Acoustic Sensors* (DAS), which is a relatively new fibre optic sensing mechanism, is rapidly spreading also because it can turn a single-mode fibre into an array of small "microphones". In this thesis a DAS system is considered. It uses a Rayleigh backscatter, in a single-mode optical fibre, as the sensing means to detect minute variations of the refractive index induced by an external acoustic wave.

2.2 OTDR

The Rayleigh-based OTDR is the preferred instrument for characterizing optical fibres. It is possible to determine losses of the interested link (splice losses, connector losses, microbending losses), distances between fibre events, links length. [2] It can be also used for sensing various perturbances that affect the light propagation along the fibre [11].
The implementation scheme of an OTDR is depicted in figure (2.4). The OTDR works as follow: a short light pulse is transmitted into the fibre under test, the

backscattered light is directed into the processing unit system in order to measure the time and the amplitude of the received signal. Since it is possible to determine the speed of the pulse as it passes down the fibre from the index of refraction, the OTDR links the backscattered received signal and the actual position in the fibre as follow:

$$z = \frac{c \cdot t}{2n} \tag{2.5}$$

In fact the OTDR receives the backscattered signal at the time instant t, when the pulse was in the position z, where n is the refractive index of the fibre, c is the speed of light. The factor two is due to the fact the pulse travel along the fibre two times: from the input to point z then the backscattered light comes back to the fibre input.

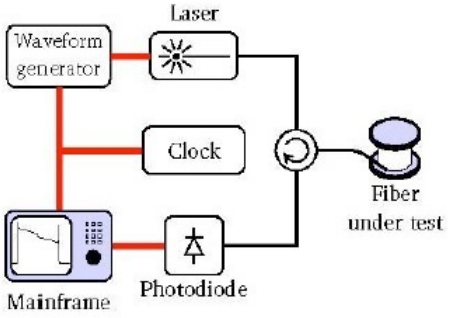

Figure 2.4: OTDR configuration scheme. There are the pulse generator system, a circulator (to separate forward light to backward signal), a photodiode and the processing system.

OTDR transforms the temporal evolution of the signal into a spatial evolution along the fibre. The received signal has been affected by an attenuation $\propto e^{-2\alpha z}$, where α is the attenuation coefficient.
Representing the power of the receiver signal in dBm, then its evolution is a straight line with a slope equal to $-2\alpha_{dB}$. OTDR represents the signal power already divided by two, in order to have the straight line slope proportional to the attenuation coefficient.
A common OTDR graph is depicted in figure (2.5). The amount of backscattered signal is proportional to the amplitude and the width of the transmitted pulse.

As has been said previously the backscattered signal has very low power, and this represent the main technical difficulty in a Rayleigh-base DOFSs [9]. Generally to overcome these problems an APD (avalanche photo-diode) is used or the measure is repeated several times and then averaged. It can be show that the SNR increase with the square root of the number of performed measures.

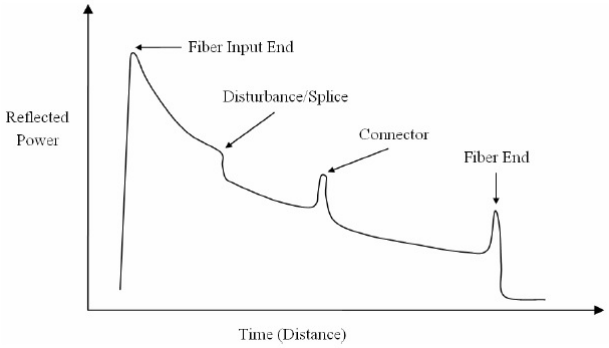

Figure 2.5: OTDR graph.

The backscattered signal power (P_d) of a fibre of length Δz (Δz has taken little enough in order to not consider losses) is equal to:

$$P_d = (S_d S_c)\Delta z P_i = S\Delta z P_i \tag{2.6}$$

where $S_d \sim \lambda^{-4}$ is the Rayleigh scattering coefficient, S_c is the capture coefficient, S is the backscattering coefficient and P_i is the power of the incident pulse when the backscattered signal originates. In addition to that the pulse backscattered power is proportional to the pulse width (Δ) in the fibre - fixing fibre properties and wavelength. A given pulse of duration τ will occupy a fibre section of length equals to:

$$\Delta = \frac{c}{n}\tau \tag{2.7}$$

The width of the pulse is not only proportional to the backscattered power but also to the measurements sensitivity: the shorter is the pulse, the sharper is the measure. One way of understanding this concept is to introduce the Minkowski diagram.

τ	10 ns	100 ns	1 μs	10 μs
$\mathbf{\Delta}$	2 m	20 m	200 m	2 km

Table 2.1: OTDR pulse width, in the fibre, related to its duration.

2.2.1 Minkowski diagram

The Minkoswki diagram shows the time and the space evolution. In figure (2.6) is shown the Minkoswki graph considering a rectangular pulse, depicted with a red line, of width OT. At the time $t = 0$ the pulse enters the fibre and the pulse head propagates along the fibre, following the line $\mathcal{L}$. During the propagation this pulse also generates backscattered light. Considering a point A in which the backscatter originates, then the back propagation will be in the direction of the segment AC. The backscattered propagation originates at time t_A and reaches the input at time $2t_A$. At the same time the end of the pulse is also propagating along the line $\mathcal{T}$, generating at the same time the backscattering phenomena. Let's consider the backscatter event that takes place at the point B. Looking at the diagram it is possible to notice that the power, measured at time $2t_A$, is the super position of the scattering generated from segment AB. This power, measured by OTDR, is equal to the scattering generated by a section of the fibre with length equal to half the transmitted pulse width. Spoken in another way, the spatial resolution of OTDR is equal to half the length of the pulse.
A brief example of the correspondence between pulse duration (τ) and its width in the fibre (Δ) is presented in table (2.1).

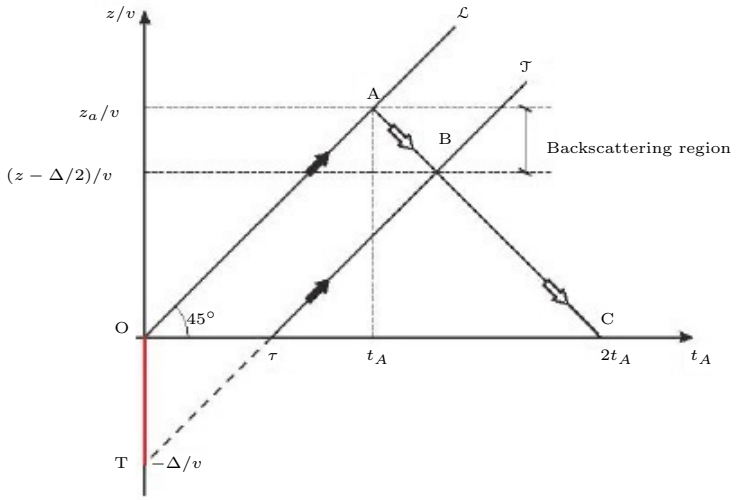

Figure 2.6: Minkowski diagram.

2.2.2 Φ-OTDR

As it has been described in the previous sections, OTDR in general it is not sensitive to phase modulation of the light. Φ-OTDR system has been designed to enhance coherent effects, and phase sensitivity as result of the interference of the backscattered light, from different points. The detection is based on the equation (2.4). With respect to OTDR, Φ-OTDR can detect perturbations much smaller than the ones perceived with a conventional OTDR [7]. In the system reported here, the phase changes result from the acoustic waves which affect the optical fibre. Φ-OTDR as the same setup as a conventional OTDR, as depicted in figure (2.4) except that the light source is a narrow-band, highly coherent laser in order to achieve the phase sensitivity that is required for this different OTDR. As seen the input is chosen coherent and then the output will be a coherent interference of different backscattered lights within the pulse width[7]. Spatial resolution of this phase sensitive OTDR, as for conventional OTDR, suffers of the same constraint on spatial resolution which is around meters. This constrain can be relaxed when the sensing is performed over a very long sensing fibre. Thus wider pulses can be used to probe the fibre also in order to increase the SNR ratio.

Φ-OTDR, in general, has been only used to measure vibrations. It is not used for perform a temperature or strain sensing because there is not a constant

relationship between the perturbation and the change of the jagged that appears. For temperature and strain sensing a mixed technique which exploit Φ-OTDR and COTDR (Coherent-OTDR) is used [1, 12].

2.3 Acoustic wave

An acoustic wave is a longitudinal wave that consists of a sequence of pressure pulses or elastic displacements of the material in which the wave propagates. When the material, in which the acoustic wave is propagating, is a solid, then the wave consists of a sequence of elastic compression and expansion waves that travel through the solid [10].
Considering and acoustic wave which is propagating, in a solid medium, along the x direction with velocity v_s, frequency f and wavelength $\Lambda = \frac{v_s}{f}$, then at position x and at time t the generated strain is equal to:

$$s(x,t) = S_0 \cos(\Omega t - qx) \tag{2.8}$$

S_0 is the amplitude, $\Omega = 2\pi f$ is the angular frequency and $q = \frac{2\pi}{\Lambda}$ is the wavenumber. Assuming the medium optically transparent with a refractive index equals to n (when there is no acoustic wave perturbation) then the refractive index can be described by:

$$n(x,t) = n + \Delta n(x,t) = n - \frac{1}{2} p n^3 S_0 \cos(\Omega t - qx) \tag{2.9}$$

The refractive index is inhomogeneous and time varying. In equation (2.9) p represents the photoelastic constant, and the term $\Delta n(x,t)$ takes into account the perturbation introduced by the acoustic wave strain [3].
In this thesis will be exploited this variation of the refractive index, caused by the acoustic wave that has to be detected, which will influence the measured quantities by the photodetector described in equation (2.4).

3

Experimental setup

The objective of this thesis is to develop an experimental DAS. This system is based on a Φ-OTDR which probes the fibre while it undergoes some perturbations by different acoustic waves. The setup that will be presented will allow to localize the positions of the acoustic waves and their frequencies.
In this chapter a description both for the experimental setups realized and for the used tools will be presented.

3.1 Experimental setup: version one

3.1.1 Source

The scheme presented in figure (3.1) represents the source of this system. It has been made by a laser, an Erbium Doped Fibre Amplifier (EDFA) and an Acoustic Optic Modulator (AOM).
The laser is a Koheras Adjustkit (figure (3.2)). It is a Distributed Feedback Laser (DFB) which differs from Fabry-Perot laser inasmuch DFB laser reflects only a narrow band of wavelengths and, this, produces only a longitudinal line. This

laser line has wavelength of 1550.02 nm, and width $< 2\ kHz$, maximum emitted power equals to 19.7 mW.
One of the requirements of Φ-OTDR is a coherent source, this is why this DFB laser has been chosen for the setup.

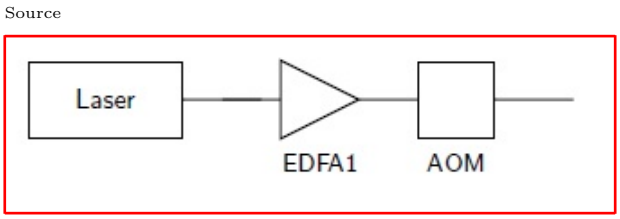

Figure 3.1: System source.

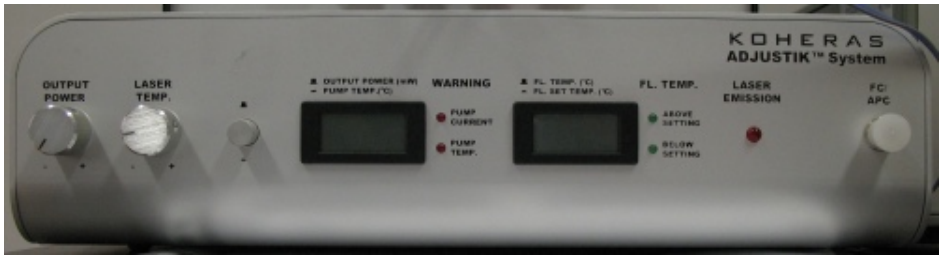

Figure 3.2: Koheras Adjustkit TAdE15PztSpM.

In some papers, also reported in this bibliography, the source part has been made by a laser followed by an AOM and then an EDFA. In this thesis this setup has been changed by flipping EDFA with AOM in order to reach a higher SNR and a lower level of noise.
Let's take the two system options with modulator and amplifier (a scheme comparison is presented in figure (3.4)) and let's analyse from a theory point of view what happens. The two different configurations will be compared using parameters as OSNR and NF.
Optical amplifiers use a doped optical fibre in order to amplify the input signal. They are very useful because they provide: an in-line amplification (without requiring electronics), have a low noise figure, have a quasi-flat gain spectrum and they are insensitive to polarization. One of the drawbacks of the EDFAs is the Amplified Spontaneous Emission (ASE) which is a noisy phenomenon due to the

amplification of photons generated by spontaneous emission. This emitted photons have phase, frequency and polarization different from the useful signal. For what concerns ASE spectrum, which is presented in figure (3.3), is very similar to the gain spectrum and the more interesting component is the one at the same frequency of the useful signal.
It can be demonstrated that the ASE power, measured along a band $\Delta\nu$, centered at signal frequency ν_s, is given by:

$$P_{ASE}(z) = 2h\nu_s\Delta\nu\eta(z) \tag{3.1}$$

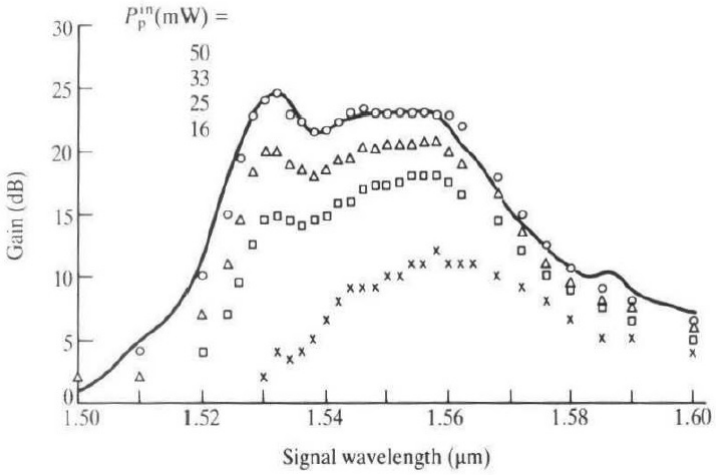

Figure 3.3: EDFA gain band.

In equation (3.1) η represents the average number of photons per ASE mode. Let's then define the optical SNR (OSNR) as the ratio between the power of the optical signal and the power of the optical noise. Then considering that an input signal with power P_{in} and frequency ν_s, affected only by quantum uncertainty, then the OSNR at the amplifier input (OSNR_{in}) and the OSNR at the amplifier output (OSNR_{out} using an amplifier gain G) will be:

$$\begin{aligned} \text{OSNR}_{in} &= \frac{P_{in}}{h\nu_s\Delta\nu} \\ \text{OSNR}_{out} &= \frac{G \cdot P_{in}}{P_{ASE} + h\nu_s\Delta\nu} \end{aligned} \tag{3.2}$$

The other parameter that will be used for the comparison is the noise figure (NF), described by (3.3), that represent the degradation of the OSNR caused by the ASE (for this specific case). Noise figure is described as:

$$\mathrm{NF} = \frac{\mathrm{OSNR}_{in}}{\mathrm{OSNR}_{out}} \tag{3.3}$$

The AOM is an instruments that introduces attenuation (A) to the signal. Let consider the following equations:

$$\begin{aligned} \mathrm{OSNR}_{A_{out}} &= \frac{AGP_{in}}{P_{ASE} + h\nu_s\Delta\nu} \\ NF_{A_{tot}} &= \frac{P_{ASE} + h\nu_s\Delta\nu}{AGh\nu_s\Delta\nu} = \frac{NF}{A} \end{aligned} \tag{3.4}$$

$$\begin{aligned} \mathrm{OSNR}_{B_{out}} &= \frac{AGP_{in}}{AP_{ASE} + h\nu_s\Delta\nu} \\ NF_{B_{tot}} &= \frac{AP_{ASE} + h\nu_s\Delta\nu}{AGh\nu_s\Delta\nu} = NF + \frac{1-A}{AG} \end{aligned} \tag{3.5}$$

As shown in equations (3.4, 3.5), which refers respectively to setup (3.4(a)) and (3.4(b)), it is possible to evince that the case AOM followed by EDFA has a bigger NF than the setup with EDFA followed by AOM. This means that the OSNR in figure (3.4(a)) has a higher value, in fact the attenuation affects, not only the useful signal, but also the ASE power.
What have been described above has been verified using the configurations depicted in figure (3.4). Data acquired are reported in table (3.1).

	$\mathbf{P_{out}}$ **[mV]**	**OSNR [dB]**
EDFA1 + AOM	185.625	26.65
AOM + EDFA1	3837	12.98

Table 3.1: Data comparison between the different setup depicted in figure (3.4).

In order to obtain data from the table (3.1) some preliminary measurements have been done. They can be summarized as follow:

1. As first measure a setup made only by the photodiode directly linked to the oscilloscope has been used (for this first part of system characterization the oscilloscope have been used as receiver. Successively it has been used the

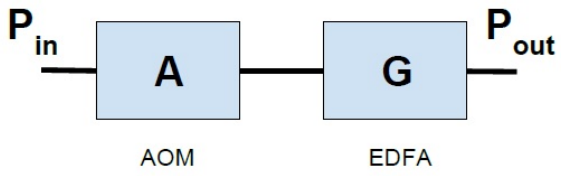

(a) case A

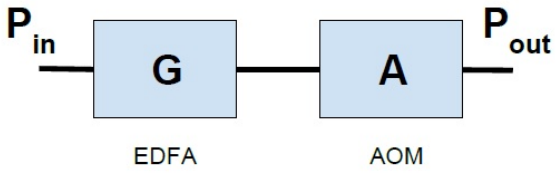

(b) case B

Figure 3.4: Different configuration using EDFA and AOM.

board PDA14). This initial measure allow to see the initial offset that has to be considered has the 0 V level.

2. The performed measures will be taken with full high power laser light. In order to avoid the photodiode saturation and that the high power level of the laser source ruins the system components is necessary to use an attenuator. For this scope have been characterized an attenuator which has an attenuation A_1= 23.98 dB.

3. Successively has been introduced the AOM and has been measured that it introduces an attenuation of A = 4.58 dB.

   - After that EDFA1 has been inserted, in the previous configuration, before the AOM and the data of the first row of table (3.1) has been obtained.
   - From the setup of described in the step (3) the amplifier EDFA1 has been inserted after the AOM and measurements have been performed in order to obtain P_{out} and OSNR - second row of table (3.1).

4. Finally the other instruments: circulator, EDFA2, filter, fibre optical coil

(named *coil 1*) have been inserted and the setup has been obtained, as depicted in figure (3.6).

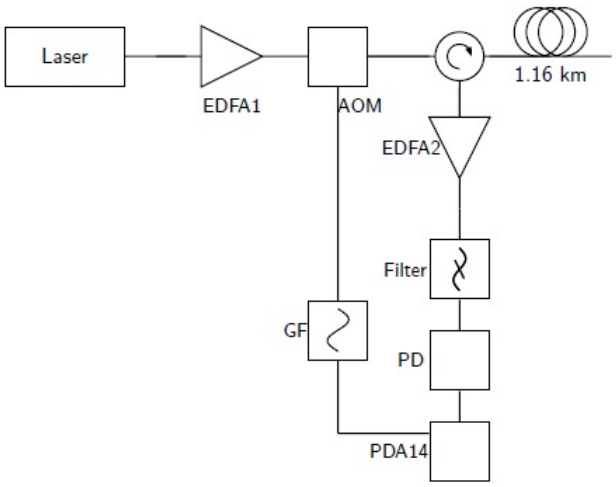

Figure 3.6: Scheme of the first setup.

3.1.2 Function Generator

This instrument, presented in figure (3.7) is used for generating the TTL signal for the AOM (using its output channel), while the sync channel is used for generating the signal used as external trigger for the PDA14. The output signal has been chosen to be a pulse wave with a chosen period T_p, and with "1" time equal to 199.850 μs while "0" time equals to 150 ns (see section 3.1.8). The sync signal is generated any time that the pulse wave period starts. In this way the PDA14 starts sampling the signal whenever it receives the external trigger (and the previous sampling operation has ended).
During sampling operation one problem is to monitor that each acquisition time is less or equal to the GF pulse wave period - for what concerning this work there is negligible percentage of lost triggers which have been measured.

In table (3.2) the GF characteristics are presented for what concern the pulse wave and the rectangular wave (rectangular wave is used in configuration presented in figure (3.12) inasmuch it is the wave with a fastest frequency period

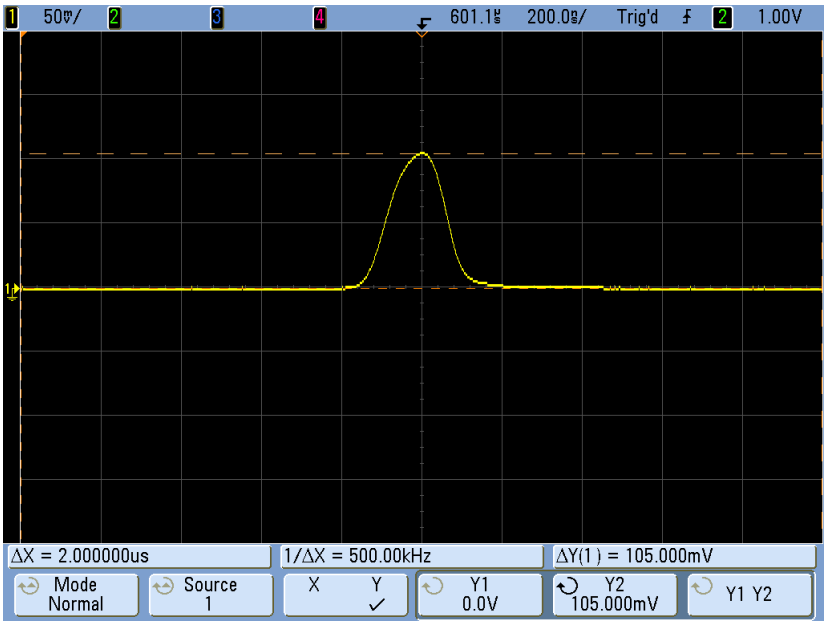

(a) Laser with 1 mW of output power liked to the AOM. Pulse width is equal to 150 ns.

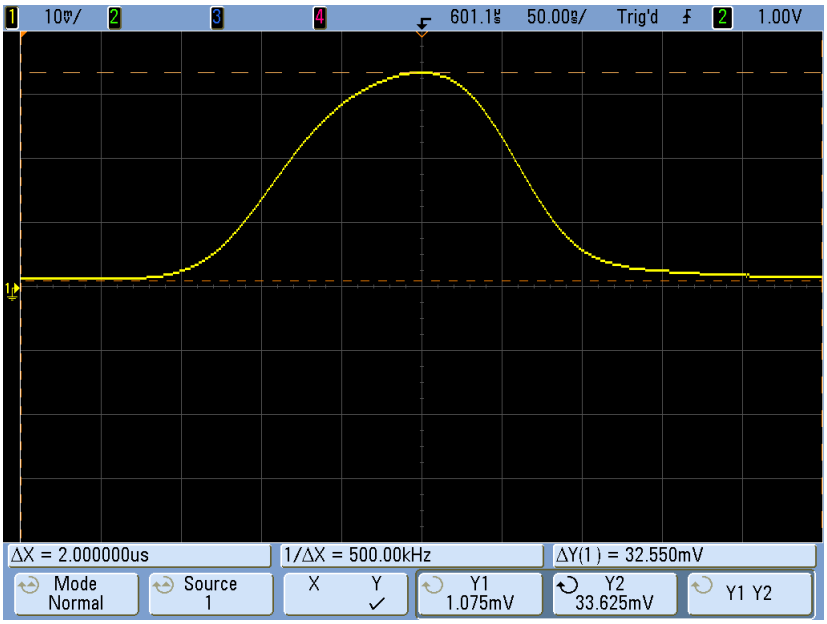

(b) Laser with 19.7 mW of output power, linked to EDFA1, AOM and the attenuator inserted.

Figure 3.5: Oscilloscope output, from different configurations.

that can be generated).

Pulse wave		**Square wave**	
Frequency range	500 μs to 50 MHz	Frequency range	1 μHz to 80 MHz
Pulse width	8 ns to 1999.9 s	Rise/Fall Time	$<8\ ns$[4]
		Duty cycle	50 % (for 80 MHz)

Table 3.2: GF characteristics for the used waveforms.

Figure 3.7: Function generator.

3.1.3 AOM

AOM, in figure (3.8) is used as a switch in order to obtain small pulses as required for Φ-OTDR. Its characteristics are listed in table (3.3). AOM needs as input the laser signal, which will be transformed in a pulsed signal, then an input of 12 V from a power supply system (Agilent E3649A) and a TTL (time to live) signal. TTL signal is generated by a FG, which sets his output as a square wave with low level equals to 0, and high level greater or equal to 600 mV. When the AOM gets a high TTL level, it outputs a low signal, and when it gets a low TTL level, it outputs an high value.

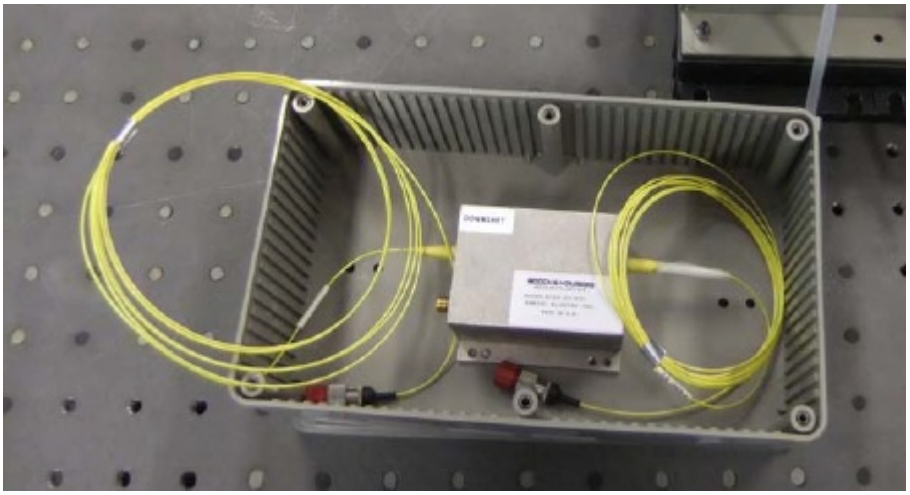

Figure 3.8: AOM.

Wavelength	1550 nm
Insertion loss	<3 dB
Estinction ratio	>50 dB
Raise/Down time	25 ns
Frequency	110 MHz
RF Power	3 W
Connectors	FC/PC

Table 3.3: AOM technical specifications.

3.1.4 EDFA

In this thesis two amplifiers has been used. The powerful one (EDFA1) has been inserted at the transmission side in order to have an initial high amplification (this is in accordance with the requirements for building the Φ-OTDR scheme). The other amplifier (EDFA2) has been positioned at the receiver side.
In table (3.4) the characteristics of the two used amplifiers are listed. While in figure (3.9) a comparison, between the two amplifiers with respect to the pump power set in the front panel of the EDFA, is presented.

	EDFA1	EDFA2
Saturated output power	18 dBm	15 dBm
Small signal gain	>35 dB	>30 dB
Noise Figure	<5 dB	<4.2 dB
Wavelength range	1528-1565 nm	1528-1565 nm
Spectral gain flatness with single channel input	0.5 dB	0.5 dB
Connectors	FC/APC	FC/APC

Table 3.4: Characteristics comparison between EDFA1 and EDFA2.

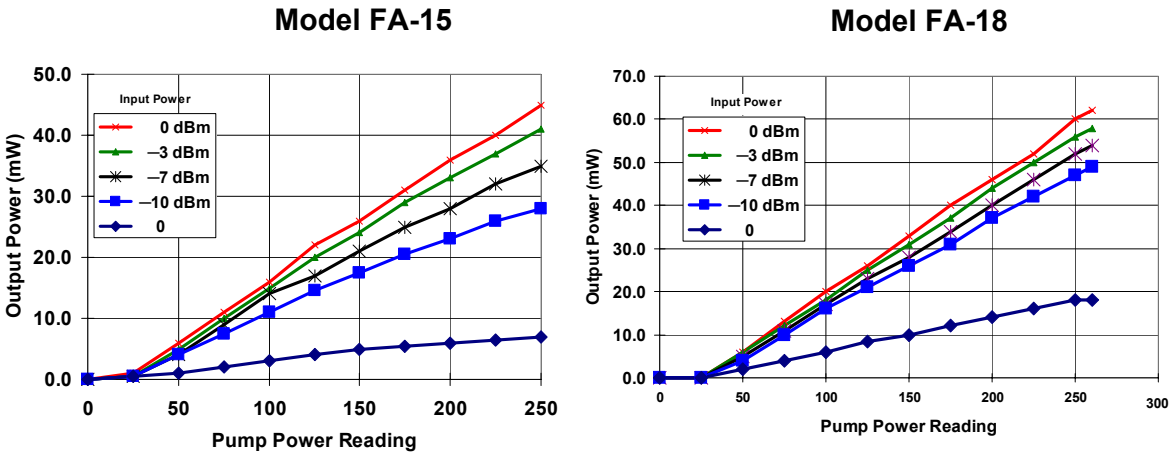

Figure 3.9: Comparison between EDFA2 (FA-15) and EDFA1 (FA-18) performances with respect to pump power.

3.1.5 Tunable grating filter

In the setup a tunable filer has been used at the receiver part. Its objective is to filter the noise (ASE) generated by amplifiers. The used filter - see figure (3.10) -

has optimized performances for the wavelength range from 1530 nm to 1570 nm. When this filter gets the light from the input fibre the internal lens collimates this source to the diffraction grating. The internal microprocessor determines how many steps the wavelength, chosen from the front panel of the filter, is far from the reference position and moves the to the required angle in order that the filtered light is then focused into the output fibre. A particularity of this filter is that all the internal filter components are bi-directional, thus the fibre ports can be independently used as input or output. This instrument, as for laser and EDFA, is temperature dependent so it is necessary, after its power up, to wait its stabilization. For what concern the stabilization of this filter there is an internal electrical current which is supplied to its heater elements until its internal temperature reaches the set point.

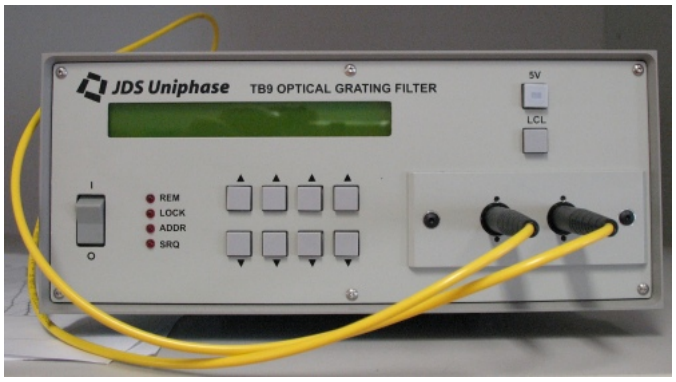

Figure 3.10: Filter: JDS Uniphase TB9022321FP3.

3.1.6 Photodiode

In order to convert light signal to an electrical signal and then measuring it using an oscilloscope or the board PDA14, has been used a photodiode HP-11982A, with conversion parameter of 300 V/W and maximum input power of 100 dBm. This instrument combines a PIN photodetector the optical input into electrical output. Before outputting the electrical signal, it is amplified with a low noise preamplifier.

3.1.7 PDA14

In order to acquire data at the output of the phtodetector, after the initial measurements which have done using the oscilloscope, the Signatec PDA14 data acquisition board has been used - see figure (3.11). PDA14 is linked to the computer and acquisition is monitored and controlled via a Matlab software. This board has three inputs:

- *Channel input 1, 2*: two input ports which are used for sampling and capturing the input signal.

- *External Clock*: it acquires that input - only if it is a sine or square wave - with frequency range in between 30-100 MHz. The signal amplitude has to be in between 100 mV p-p and 2.0 V p-p. It is possible also to use PDA14 internal clock which provides rates into a range from 100 MHz to 976 kHz in factors of 2, with an accuracy of ± 0.01 %.

- *External trigger*: is used for triggering the board in order to can catch the input signal. The user can also decide to use a different trigger source taken from input channel 1 or input channel 2; which are considered as internal trigger. If the user decide to select an external trigger, the board will take the sync signal from this input port. A trigger parameter that has been set is the *trigger level*. This parameter defines the amplitude at which the trigger will occur. A trigger signal is considered valid when it passes through the defined trigger level, in the direction set by trigger slope.
  In this thesis, an external trigger is used - it is provided by the functions generator. The external trigger can be set using a value range between $[-1.75,\ 1.75\ V]$. The PDA14 is set in post-trigger mode, in this way the trigger signal is used as starting point for the data acquisition.

- *Digital output*: this connector can supply some of the digital signals that may be used for synchronizing external events or to monitor internal processes.

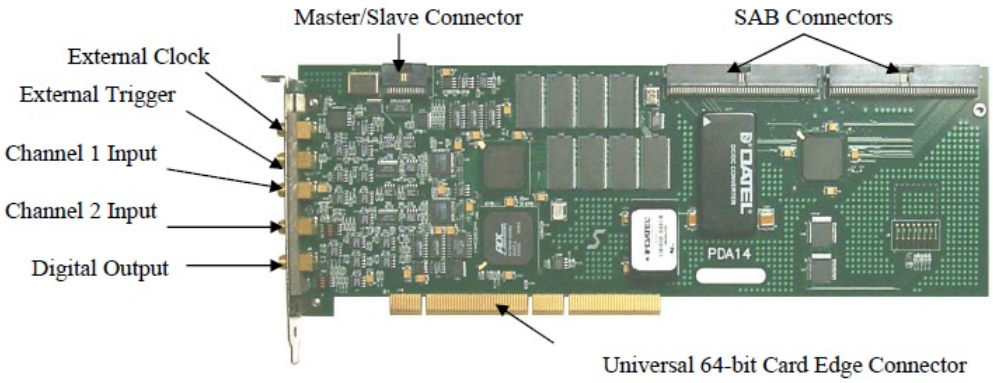

Figure 3.11: PDA14 board.

The PDA14 board is linked to the computer via the PCI port. For this work the PCI transfer mode has been set. In table (3.6) are summarized some of the PDA14 characteristics [15], while in figure (3.13) is depicted the blocks diagram of the PDA14. In this work only one analogical input channel has been used, and the total available PDA14 RAM memory space is of 512 MB, divided by two blocks FIFO 4K x 32 bit. The digitalization rate is used as set by default, at 100 MHz. While the PCI bus transfers data with a rate of 266 MB/s.
For what concerning the acquisition part, PDA14 RAM can be used both as a target for acquisition data and as a large FIFO when big amount of data are transferred over the PCI bus. For what concerning this work RAM is used as a big FIFO memory. PDA14 transfers data over the PCI bus exploiting Direct Memory Access (DMA) transfers which is a contiguous, non-paged space of memory. First of all DMA buffer has to be allocated, after that DMA can be used for transferring bunches of data at a theoretical rate of 266 MB/s.

3.1.7.1 PCI acquisition mode (with buffer)

As mentioned before PCI acquisition mode has been set for this work. PDA14 provides different kinds of acquisitions. In order to choose the one that fits better for this system, an acquisition test has been performed. The used scheme is depicted in figure (3.12). In this configuration two GFs has been connected to the PDA14: GF_1 has been connected to the trigger connector, while GF_2 has

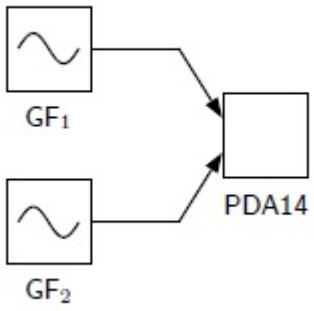

Figure 3.12: Scheme used in order to evaluate acquisition speed of the various acquisition PDA14 methods.

been connected to the channel 1 input. The objective is to evaluate the minimum acquisition time, for each of the acquisition functions proposed by the board, in order to choose the fastest acquisition method. In order to do that, FG_1 has been set to provide a trigger signal, with the fastest possible period with respect to FG characteristics. The period of the trigger signal is set to 12.5 ns. In this way the board at each trigger period acquire the FG_2 signal for a specified number of samples - this number of samples chosen to be acquired is 2048 and 4096 (details about calculations will be explained afterwards). Signal generated by FG_2 is a sine wave with infinite time duration. Data are summarized in table (3.5) where it is possible to see as PCI buffered transfer mode is the faster, compared with the other acquiring methods. Buffered acquisition is set in order to transform the entire RAM as a giant FIFO, to prevent data from being lost.

Number of samples	**AcquireToBoardP14( ) + BoardToPcP14( ) [ms]**	**AcquireAnd TransferP14( ) [ms]**	**AcquireTo PciP14( ) Buffered mode [ms]**
2048	0.298	0.122	0.089
4096	0.333	0.160	0.119
6144	0.41	0.23	0.150

Table 3.5: PDA14 acquisition functions average time using 10^5 iterations.

Analog Inputs ch1, ch2	
Full scales voltage ranges (p-p)	200 mV, 333mV, 600 mV, 1.00 V, 1.60 V, 3.00 V
Impedance	50 Ω
Bandwidth	100 MHz
Coupling	AC or DC
External Trigger	
Signal type	Sine or square waves
Impedance	1 $K\Omega$
Trigger Level	± 1.75 V
Bandwidth	50 MHz
Coupling	DC
Memory	
Active Size	256 MSamples
Addressing	DMA transfer from starting address
SampleSize	8 or 16 bits

Table 3.6: Characteristics of the board PDA14.

3.1.8 Calculations

The used coil is a single mode reduced fibre (SM-R) conform to ITU-T G.652. This fibre as an attenuation of $\alpha_1 \sim 0.2\ dB/km$ for $\lambda = 1550\ nm$. Its length is equal to $L_1 = 1.16\ km$. These characteristics have been verified using an OTDR.

Then the Round Trip Time (RTT) from the source, going along the connections fibre and continuing to the fibre coils and coming back is given by:

$$RTT = \frac{2Ln}{c} \tag{3.6}$$

L represents the total length and it is given by $L = L_f + L_1$ where $L_f \cong 10\ m$ is the length of the all optical cables between the laser source and the *coil 1*, and $L_1 = 1.16\ km$ is the length of the *coil 1*. Then $c = 3 \cdot 10^8\ km/s$ represents the speed of light in the vacuum, while $n = 1.5$ is the refractive index of the fibre.
Considering the characteristics of the PDA14 board (using the default digitalization rate[1]), and that the number of samples (ns) for an acquisition of length "duration" $[\mu s]$ is given by:

$$ns = \left\lceil \frac{\text{duration}}{2^{\text{clockDivider}}/100} \right\rceil_{2048} \tag{3.7}$$

As consideration it is necessary to say that ns, as required by PDA14 board, has to be a multiple of 2048. Then with $RTT = 11.7\ \mu s$, the time duration for the acquisition has been chosen equals to 20 μs, which entails a number of samples acquired $ns = 2048$.

Then it is necessary to take into consideration that the pulse period (T_p), generated by the source, has to be greater or equal the $\max(RTT, func\ time)$, where *func time* represents the average time measured for acquiring data with the PDA14 with the chosen acquisition function in this case is AcquireToPciP14() (buffered). For what concerning this setup it holds that:

$$T_p \geq RTT, \quad T_p \geq \text{func time} \longrightarrow T_p = 200\ \mu s \Leftrightarrow f_p = \frac{1}{T_p} = 5\ KHz \tag{3.8}$$

The objective is to acquire several measurements (M) from the fibre, each of one of length 20 μs or equivalently ns = 2048 - the arrangement of the various

[1] It leads to a sampling interval of 2 m. While the spatial resolution depends on the transmitted pulse width.

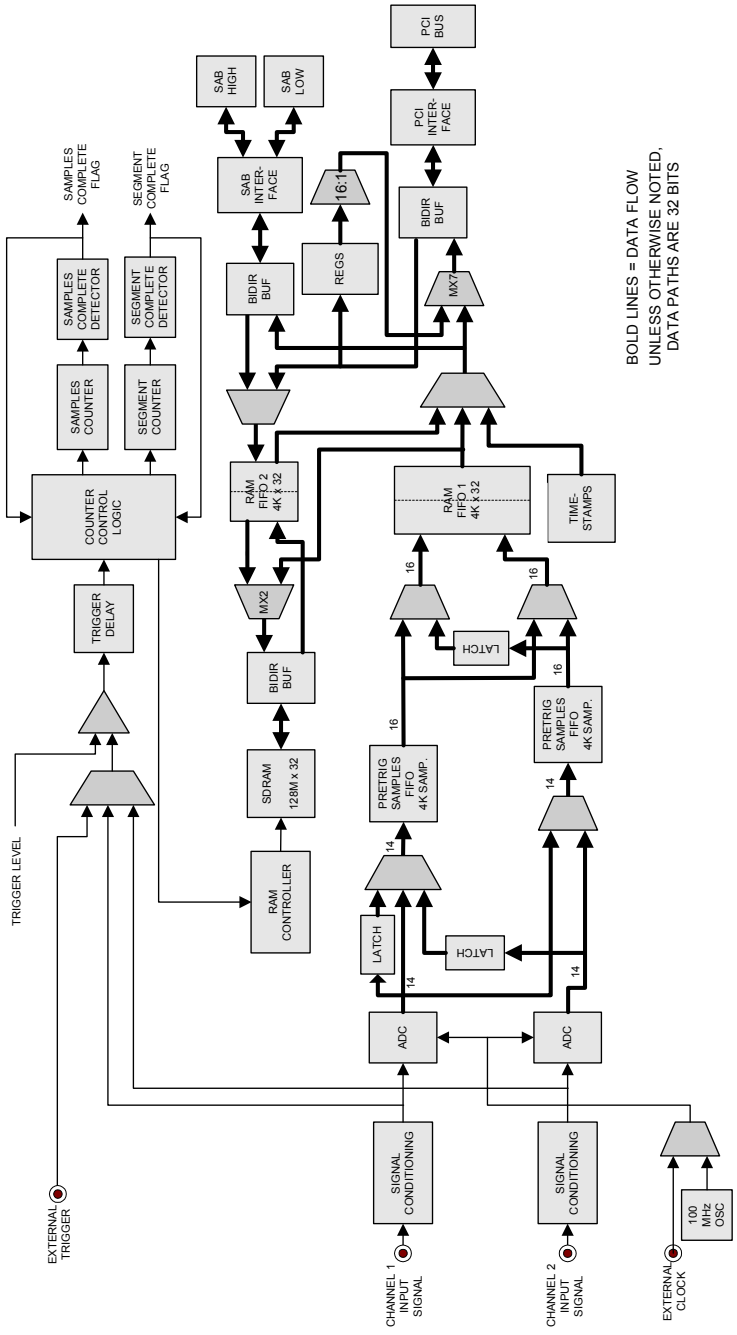

Figure 3.13: PDA14 components blocks diagram.

measurements is depicted in figure (3.14). These measurements correspond to sample the fibre at a frequency 5 kHz which has to be (for Nyquist theorem) $\leq 2f_{ac}$ that is the frequency of the perturbation that has to be measured. In this case this perturbation is given by the acoustic wave. For the considerations written above then $f_{ac} \leq 2.5\ kHz$.

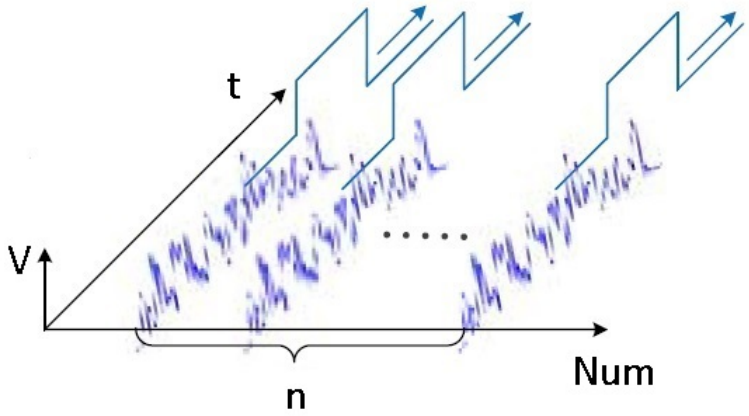

Figure 3.14: Acquisitions arrangement graph. n represents the various acquisitions, t is the acquisition time, which can be converted also in a spatial measurement, and V represents the amplitude of the measurements.

All the n measurements performed are stored in a matrix **M** (**m**x**n**), where m is equal to the number of samples acquired in the i-th acquisition.
Rows are samples and they correspond to a measurement of length, along the fibre length (z). While columns are the various acquisition performed, each of them corresponds to an acquisition spaced by T_p from the precedent one: these are time measurements (t).
During the perturbation with the acoustic wave - generated by the computer and amplified by an acoustic amplifier - the refractive index and s_{ij} change periodically and this causes a periodically change in $P(t)$ (considering equation (2.4)). Each power measurement is perturbed by acoustic wave, only in the portion of fibre which the perturbation act. For this reason, using a Fast Fourier Transform (FFT) for each position, is possible to identify frequency and location of the acoustic perturbation.
A representation of **M** and its FFT is presented in figure (3.15).

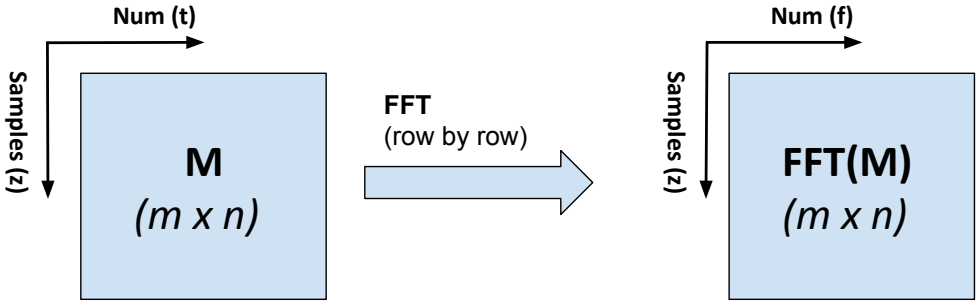

Figure 3.15: Representation of matrix **M** and its FFT.

3.1.9 Pulse Width

One of the parameter that has to be set in order to acquire data is the pulse width. This is an important parameter which affects the backscattered power, as shown in equation (2.6). The fibre section Δz, in which the backscattered propagation originates, corresponds to the pulse length in the fibre - see equation (3.9) in which has been exploited equation (2.7).

$$\Delta z = \frac{1}{2}\frac{c\tau}{n} = \frac{\Delta}{2} \tag{3.9}$$

Pulse width affects also the signal to noise ratio in fact taking into consideration a halve pulse width, it means that the backscattered power is halved as well. Then considering that the receiver band has to be larger enough to fit the pulse band, it means that reducing by a factor two the pulse width (and increasing the spatial resolution), the receiver bandwidth will be doubled. This cause a redouble of the noise power.
Summarizing, if the objective is to increase the spatial resolution of the measure this will reduce the signal to noise ratio, e.g. halving the pulse width, this will double the spatial resolution but will decrease the SNR by a four fold factor.
In this work has been chosen a pulse width equals to 150 ns which leads to a spatial resolution of 15 m, while the sample resolution is equal to 1 m.
Considering the first setup - see section (3.1) - where the Φ-OTDR trace can be

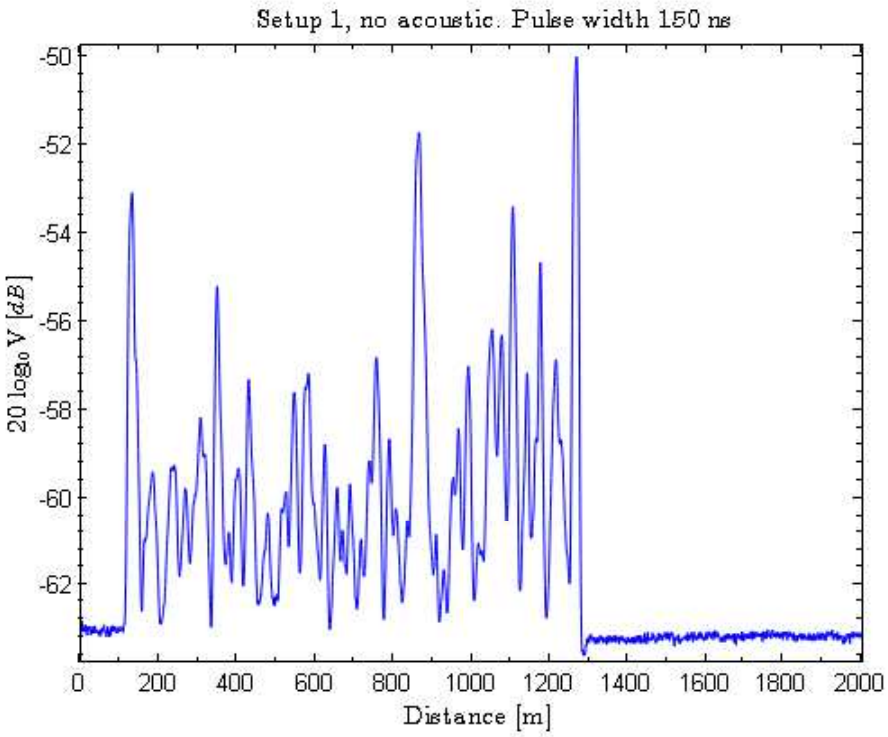

Figure 3.16: Trace, of the first setup, obtained as output at the PDA14.

seen in picture (3.16), has been practically proven the equation(2.6), where with the increasing of the pulse width the backscattered power increases as well (this will lead to a degradation of the signal to noise ratio). In figure (3.17), different measures have been overlapped, and it is possible to see that the *green* trace has an average power higher than the *black* trace. In addition to that, the green trace has a bigger resolution; this clarifies why the detected events with the pulse width of 500 ns are less noticeable with respect to the measures performed using a lower pulse width.

3.2 Experimental setup: version two

This setup is similar to the one described in section (3.1), with the addition of another coil (*coil 2*) linked at the end of the *coil 1*. A scheme of this configuration

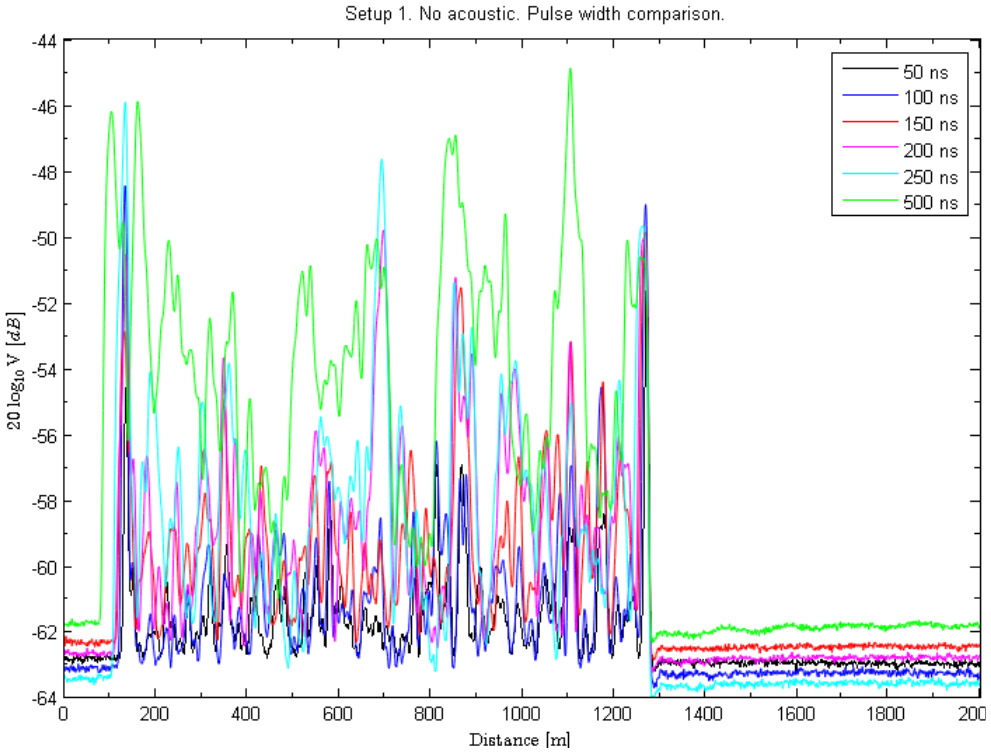

Figure 3.17: Different traces, of the setup 1, obtained varying the pulse width. The measured traces with a bigger pulse width, have both a bigger resolution - in fact detected events along the fibre setup are less emphasized with respect to the trace obtained using a smaller pulse width - and bigger averaged backscattered power.

is presented in figure (3.18).

With this new configuration the amplifier of the first setup and a loudspeaker have been used. As in the previous setup the amplifier has the role of amplifying the given wave, generated through the computer, while the loudspeaker generates the wave through a GF_2. The two waves affects the two coils and in order to avoid the acoustic interference between the two acoustic perturbations, each coil and its perturbation have been isolated using a two carton boxes.

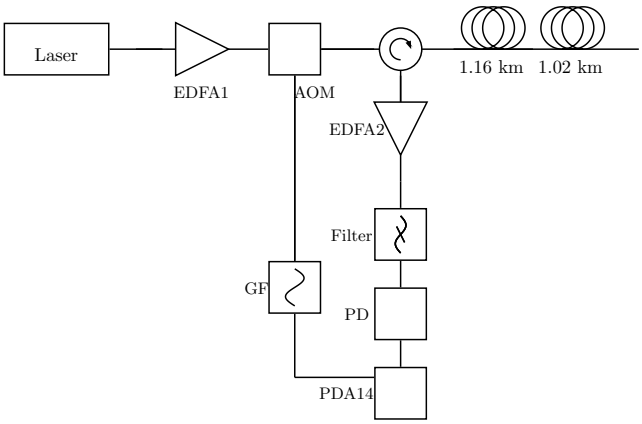

Figure 3.18: Scheme of the second setup.

3.2.1 Calculations

The new coil is a a single mode reduced fibre (SM-R) conform to ITU-T G.652. This fibre as an attenuation of $\alpha_2 \sim 0.2\ dB/km$ for $\lambda = 1550\ nm$. Its length is equals to $L_2 = 1.02\ km$. These characteristics have been verified using an OTDR. In this case the total length $L = L_f + L_1 + L_2 = 2.19\ km$. Using equation (3.6) RTT is equal to 21.9 μs. In this case "duration" has been chosen to be 30 μs which, using equation (3.7), corresponds to acquire 4096 samples.
Exploiting table (3.5) and the fact that $T_p \geq \max(RTT, func\ time)$ then can be still used the equation (3.8).

3.3 Experimental setup: version three

This setup is very similar to the one described in section (3.2). In this case has been added a new coil (*coil 3*) after *coil 2* and then in the link between *coil 1* and *coil 2*, and between *coil 2* and *coil 3* has been used a fibre linkage of around 10 m.
Then the two fibre linkages have been perturbed using for both the same amplified acoustic wave generated at a given frequency. In this case the objective is to detect the acoustic wave perturbation confined in the two spots of the setup. The third setup is depicted in figure (3.19).

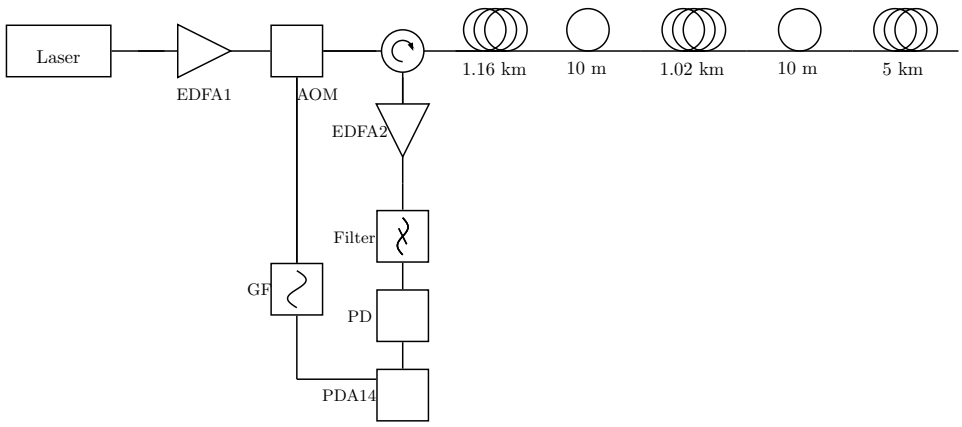

Figure 3.19: Scheme of the third setup.

3.3.1 Calculations

The total length is equal to $L = L_f + L_1 + L_{10} + L_2 + L_{10} + L_3 = 7.21\ km$, where $L_3 = 5\ km$ is the length of the *coil 3* and $L_{10} = 10\ m$ is the length of the linkage between coils 1 and 2 and between coils 2 and 3. *Coil 3* has an attenuation of $\alpha_l \sim 0.25\ dB/km$ (for $\lambda = 1550\ nm$) and it is a single mode fibre. These measurements has been performed with an OTDR.
Using equation (3.6) RTT is equal to 73 μs. For this calculation has been chosen total length of the setup of 7.30 km.
In this case "duration" is chosen to be 80 μs which, using equation (3.7), corresponds to acquire 6144 samples. Exploiting table (3.5) and the fact that

$T_p \geq \max(RTT; func\ time)$ then the equation (3.8) becomes:

$$T_p \geq RTT, \quad T_p \geq \text{func time} \longrightarrow T_p = 250\ \mu s \Leftrightarrow f_p = \frac{1}{T_p} = 4\ kHz \tag{3.10}$$

In the equation (3.10) has been chose a value of T_p equals to 250 μs in order to have a $\sim$ 100 μs of a gap with respect to the theoretical calculated value.
Due to the changing of the T_p period will change the maximum acoustic wave detectable. As described above, the measurements correspond to sample the fibre at a frequency 4 kHz which has to be (for Nyquist theorem) $\leq 2f_{ac}$ that is the frequency of the perturbation that has to be measured. For these considerations then $f_{ac} \leq 2\ kHz$.

4

Results

In this chapter the results, obtained with different setups previously described, will be presented.
This chapter is organized in three different sections, one for each tested setup. For each section at the beginning will be presented the trace measured, in the time varying domain, and successively is presented this trace in the frequency domain in which the acoustic wave, at a given frequency is highlighted.
As described in the previous chapter the used pulse width is of 150 μs, while the number of acquisitions, in one measurement session, is equal to 1000 (the number of acquisitions is the same for each setup). These considerations are true for all of the following measurements.

4.1 Setup 1

This setup has been realized as depicted in figure (3.6). The measured trace is presented in figure (4.1(a)), in which it is possible to identify the events that characterize this setup. The two interesting events are presented by the first and the last big peaks which represent respectively the start point and the end point

of the fibre under test. At the end of the fibre has been added a rolled fibre connector, in order to highly attenuate the last peak. That's why at the end there is an attenuation, followed by a small event of insertion loss.
The trace results is not very smooth because it is affected by the noise.
In addition to that it is possible to see the length of the used coil, which is $\sim 1.16\ km$, and this section is presented in figure (4.1(b)). The red line represents the best approximation, of the blue line, using the Least Square Approximation (LSA) method. Exploiting this approximation is possible to calculate the attenuation of *coil 1* which is $\alpha \sim 0.25\ dB/km$. This value is very similar to the value read on the coil label.

When the acoustic perturbation is not applied, some "unexpected" peaks at the frequencies around 1 kHz, can be detected in the signal spectrum. These peaks are noise generated by the two EDFAs in the system: in fact measuring the noise of only the PD and the PDA14, the obtained spectrum is cleaned and no unexpected lines are detected. For this reason it is possible to understand that the noise can only depends on the optical amplifiers.
In the pictures (4.2(a)), 4.2(a)) the spectra, of the measured traces which has been obtained after averaging all the traced obtained in one measurement session, is depicted - it means that the average has been performed along the *Num (f)* direction of the matrix **M**: figure (3.15).

When the acoustic wave perturbation is activated along all the *coil 1* then can be seen in the spectrum that at the given frequency appears a peak, as expected - see figure (4.2(b)). With this graph acquired information is that the distributed sensor is perturbed by an acoustic wave at the given frequency. It is not enough inasmuch it would be more useful to see just a peak at the given acoustic frequency, while the rest of the spectrum is nearly flat. In this way is immediate to understand where is the acoustic frequency. For this reason the concept of Power Spectral Density (PSD) has been introduced. Exploiting (4.1)[1] the PSDs, for both the signals with and without the acoustic wave perturbation, has been calculated. Then subtracting the two PSDs a peak at the given perturbation frequency has to appear. These measurements are affected by different kinds of noise and for this reason it is necessary to use the LSA method to better

[1] In this equation $x(k)$ is a Wide Sense Stationary (WSS) process, $r_x(n)$ is the autocorrelation function. That relation holds if $\sum_{n=-\infty} \infty |n| r_x(n) < \infty$

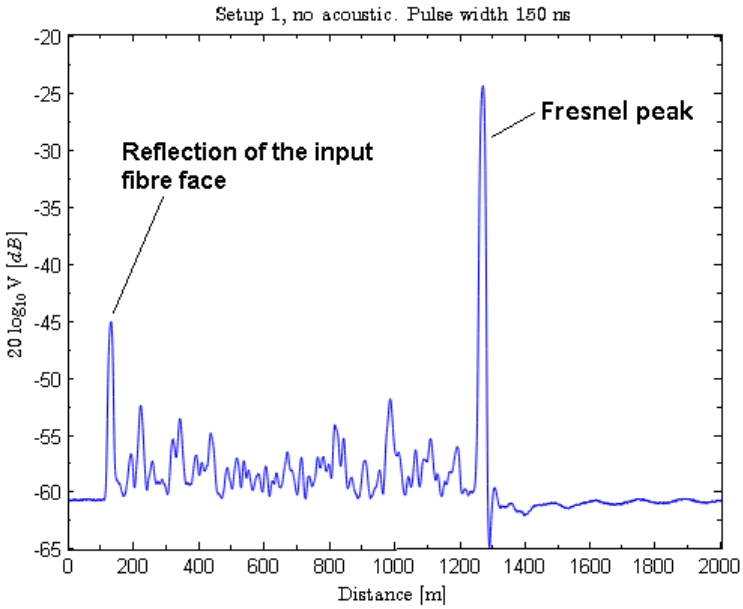

(a) Trace, with identified events, of the first setup.

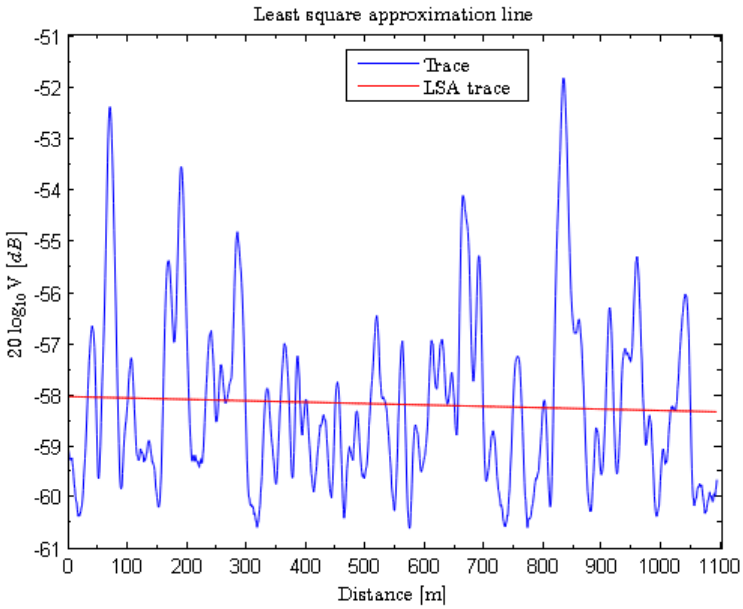

(b) Part of the trace ($\sim 1.16\ km$) of the first setup (only the *coil 1* samples, except for the input and output peaks) in which has been applied the Least Square Approximation (LSA) method in order to reduce the uncertainty of the measure for the attenuation α.

Figure 4.1: Measured trace of the first setup.

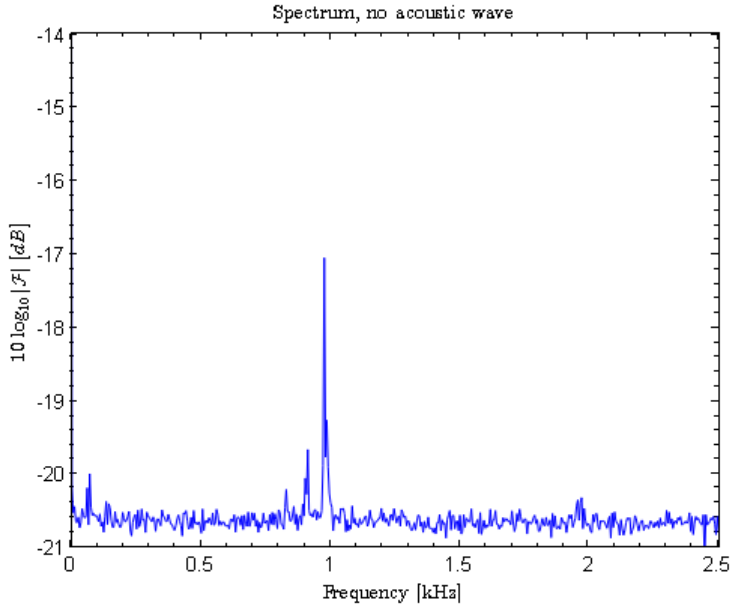

(a) Spectrum of the setup 1 trace, without the acoustic wave perturbation.

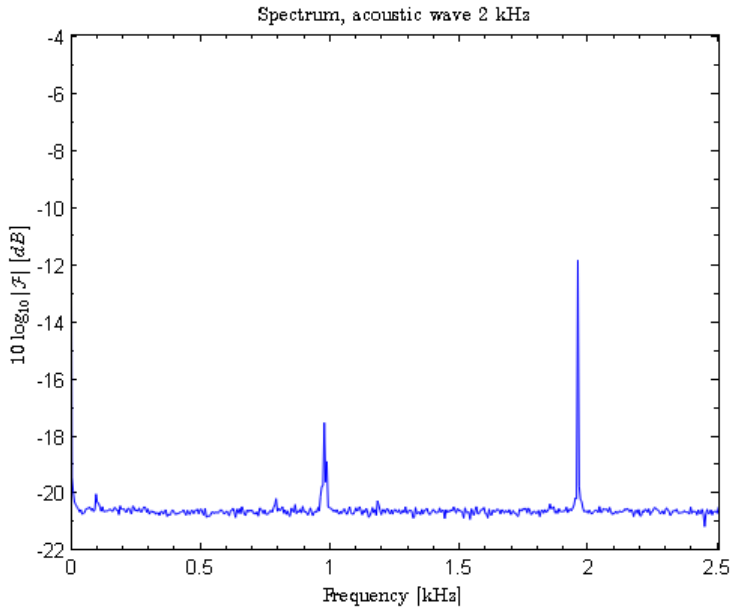

(b) Spectrum of the setup 1 trace, with the acoustic wave perturbation at 2 kHz.

Figure 4.2: Spectrum of the first setup measure.

understand the curve trend.
What has been described can be observed in figures (4.3(a),4.3(b)). In figure (4.3(a)) can also be observed some lobes at the first frequencies. It is not a strange result. It depends on the performed FFT which introduces that phenomenon called spectral leakage.

$$\mathcal{P}_x(f) = T_c\mathcal{F}[r_x(n)] = \lim_{K\to\infty} E\left[\frac{1}{KT_c}\left|T_c\sum_{k=0}^{K-1} x(k)e^{-j2\pi fkT_c}\right|^2\right] \tag{4.1}$$

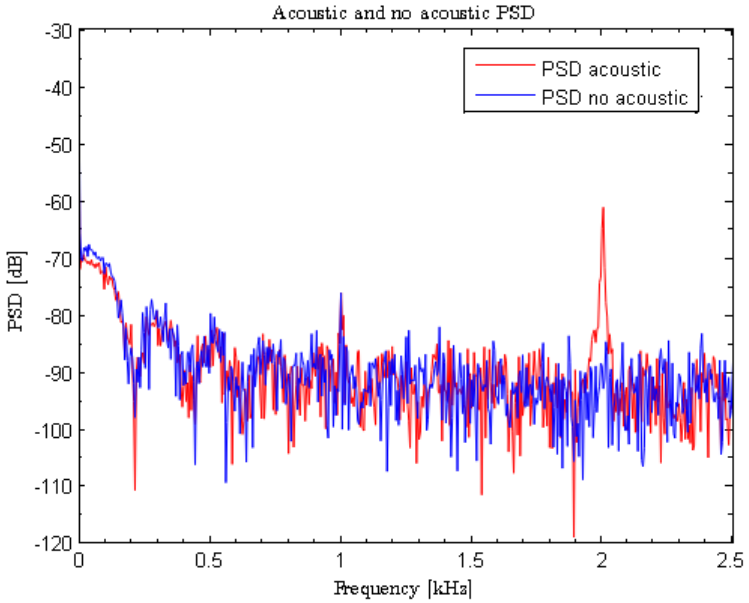

(a) Overlapped PSDs of the two measured traces (with acoustic wave at 2 kHz and without acoustic wave).

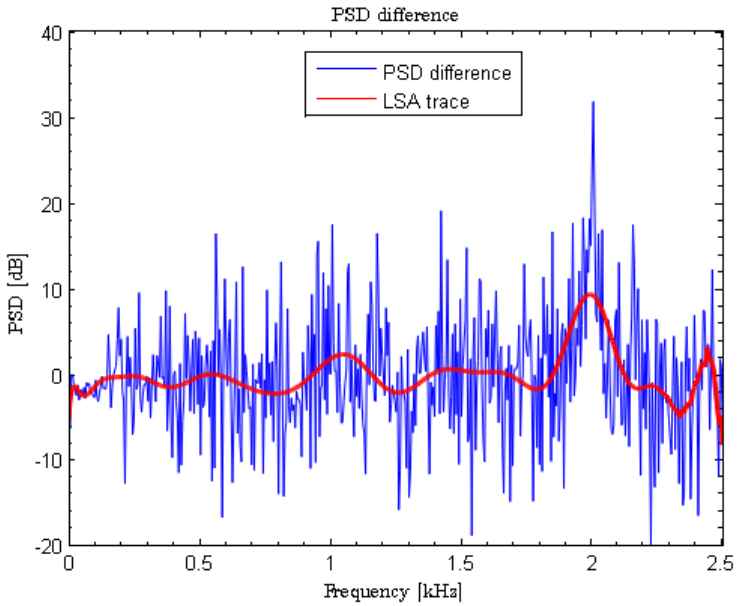

(b) Difference of the two PSDs (with and without acoustic perturbation). The red line represents a LSA curve in order to highlight that the PSD peak is around the given frequency of 2 kHz.

Figure 4.3: PSD of the first setup.

So far the information that can be obtained, only looking at spectrum of the measures, has been described. Exploiting matrix **M** a double information can be obtained, both the frequency at which the acoustic wave is working and where is precisely located along the fibre length.
In figure (4.4) is depicted a map in which at the frequency of 2 kHz for all the length of the fibre there is the acoustic wave perturbation. In this graph it has been considered only the part of the fibre in between the peaks of start fibre and end fibre, and has been deleted the noise component around the 1 kHz. As expected at 2 kHz has been detected the acoustic line, which is for the first 700 m with a higher intensity then the remaining part of the fibre. To explain this phenomenon let's consider a coil; it has one connector which is linked to the external fibre, while the other connector is linked to the inner fibre of the coil. During the measurements, the amplifier has been arranged in front of the coil. The acoustic wave mostly perturbed the external fibre of the coil (the first 700 m) and with lower intensity it has affected the inner fibre of the coil.
In the first part of the fibre length there are some points which have higher intensity of the others. It happens because the acoustic wave affected only one side of the fibre, and the region closer to the perturbation got a higher level of acoustic wave intensity level.
In figure (4.5) is depicted the three dimensional view of the graph in figure (4.5) in order to give a better perception of the acoustic wave effect along the fibre.
These two aforesaid graphs have been obtained after applying the moving average - see equation (4.2)[1] - of the matrix **M**. Has been request to do this operation due to the fading noise which generates some fluctuations of the total intensity and preventing the clear localization of the acoustic wave frequency.

$$R_i = \frac{1}{V} \sum_{l=i}^{l=i+V-1} r_l, \quad l \in [1, N], \quad i \in [1, N - V + 1] \tag{4.2}$$

[1]Supposed that there are N acquisitions, in one measurement session, V is the moving average number, r_i is one acquisition trace and R_i is its averaged trace.

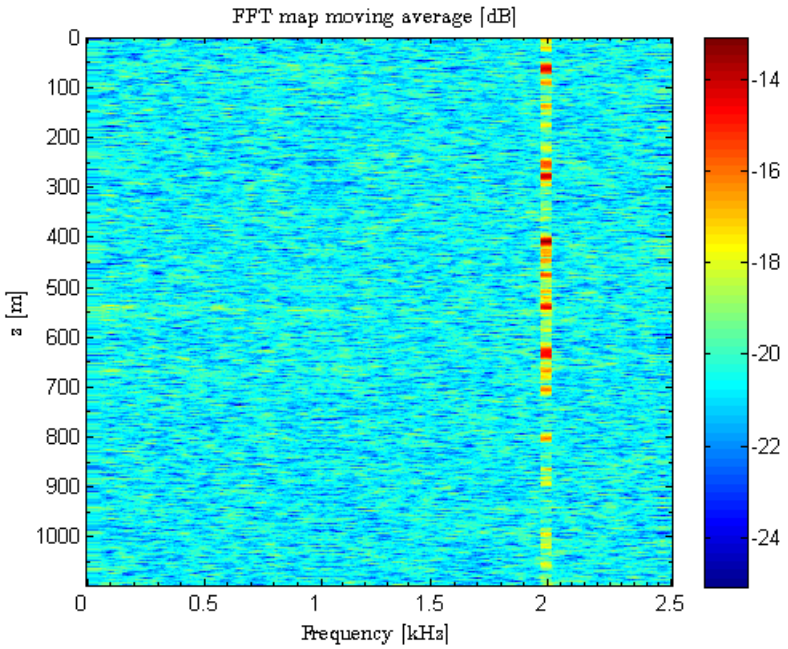

Figure 4.4: Representation of matrix $\mathcal{F}(\mathbf{M})$ in dB units.

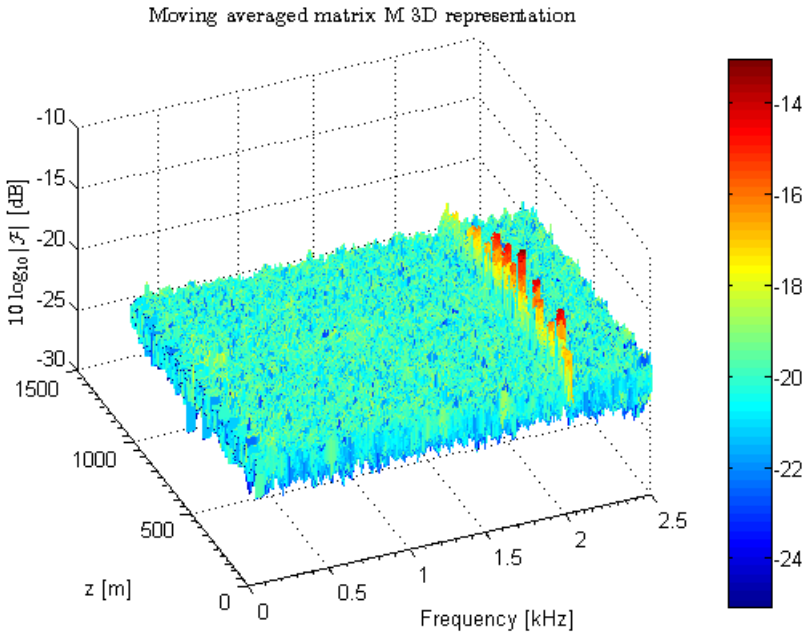

Figure 4.5: Representation of matrix $\mathcal{F}(\mathbf{M})$ as a 3D graph, in dB units.

4.2 Setup 2

This setup has been realized as depicted in figure (3.18). The measured trace is presented in figure (4.6(a)), in which it is possible to identify the events that characterize this setup. The first peak represents the reflection of the input fibre face (of the first coil), while the second peak (located at the end of the first fibre and at the beginning of the second fibre) can be interpreted as the union between the *coil 1* Fresnel peak and the *coil 2* initial reflection peak. The last peak is the *coil 2* Fresnel peak. In that position can be seen that there is not only a reflection loss but also an insertion loss; this is due to the insertion of a rolled fibre connector, at the end of the setup - in order to avoid a big end peak which could badly affect the measurement instruments. In addition to that it is possible to see the length of the used coils, which correspond to a total of $\sim 2.20\ km$. As have been done in setup 1, here has been applied the LSA method in order to calculate the fibre attenuation. In figure (4.6(b)) is depicted only the *coil 2* measurements, in blue, and, in red, the first order LSA line. In this case the attenuation for *coil 2* is $\alpha \sim 0.26\ dB/km$, which is similar to the value read on the coil label.

As described in the setup 1, also in this configuration, there are some noise frequencies near 1 kHz - see figure (4.7(a)). The following figures about the spectra of the measured traces has been obtained after averaging all the traced obtained in one measurement session - it means the average has been performed along the *Num (f)* direction, if it is considered the matrix $\mathbf{M}$: figure (3.15).

In this case has been used two acoustic waves (one at 1.5 kHz and another at 2 kHz), one has been generated in order to affect one coil and the other in order to affect the other coil. In the spectrum of figure(4.7(b)) the two peaks at the given frequencies can be easily seen. For the same reason described for setup 1, also here has been calculated the PSD. Due to the fact that in this setup there are two different perturbations, located in two different coils then it is necessarily to calculate two different PSD: one for the first coil and another for the second coil. In figure (4.8(a)) can be seen the two overlapped PSDs, and as expected there are the two peaks at the acoustic waves frequencies.
Successively have been performed two subtractions: one between the PSD, obtained by the measure without the acoustic perturbation, and the PSD of the first

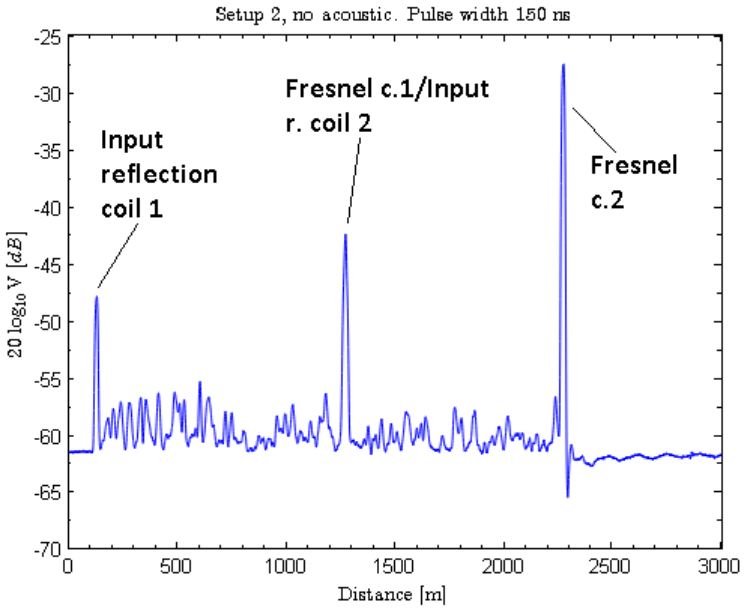

(a) Trace, with identified events, of the second setup.

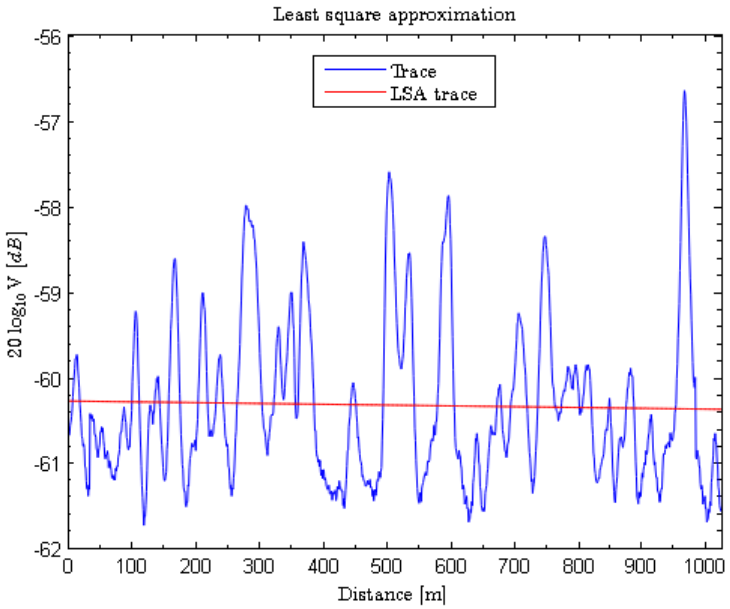

(b) Part of the trace ($\sim$ 1.02 km) of the second setup (only the *coil 2* samples, except for the input and output peaks) in which has been applied the Least Square Approximation (LSA) method in order to reduce the uncertainty of the measure for the attenuation α.

Figure 4.6: Measured trace of the second setup.

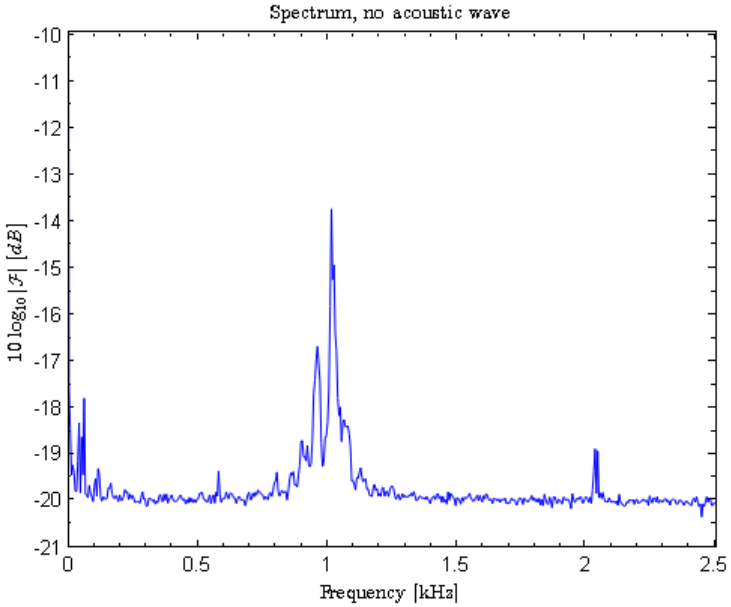

(a) Spectrum of the setup 2 trace, without the acoustic wave perturbation.

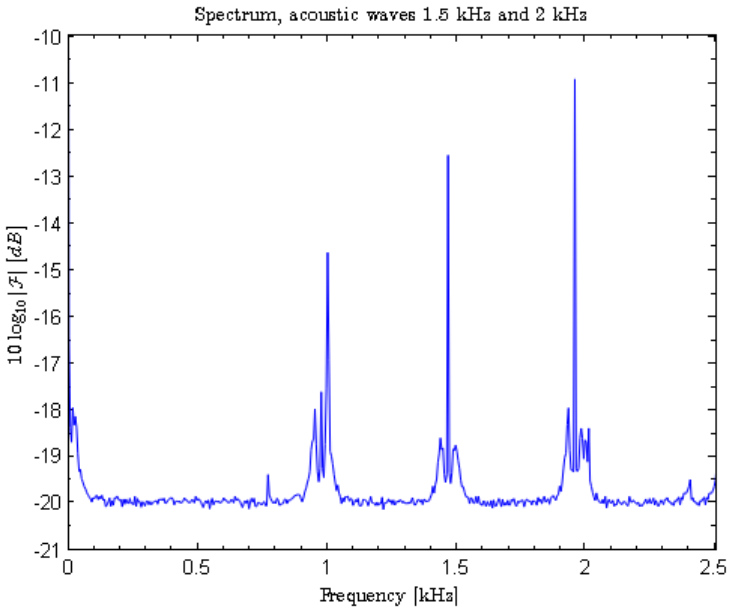

(b) Spectrum of the setup 2 trace, with the acoustic waves perturbation at 1.5 kHz and 2 kHz.

Figure 4.7: Spectrum of the second setup measure.

coil measure, and another subtraction between the PSD of the measure without the acoustic perturbation and the PSD of the second coil. In figure 4.8(b)) can be seen the two approximated curve (red and yellow) which represents the performed subtractions. As expected the two acoustic frequencies peaks has been detected. Also in this case, in figure (4.8(a)) can also be observed some lobes at the first frequencies due to the spectral leakage.

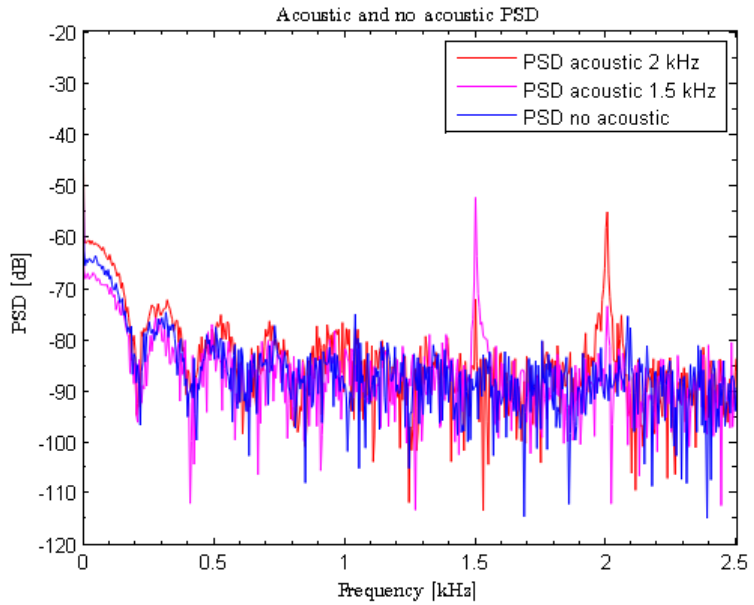

(a) Overlapped PSDs of the two measured traces (with acoustic waves at 1.5 kHz and 2kHz and without acoustic wave).

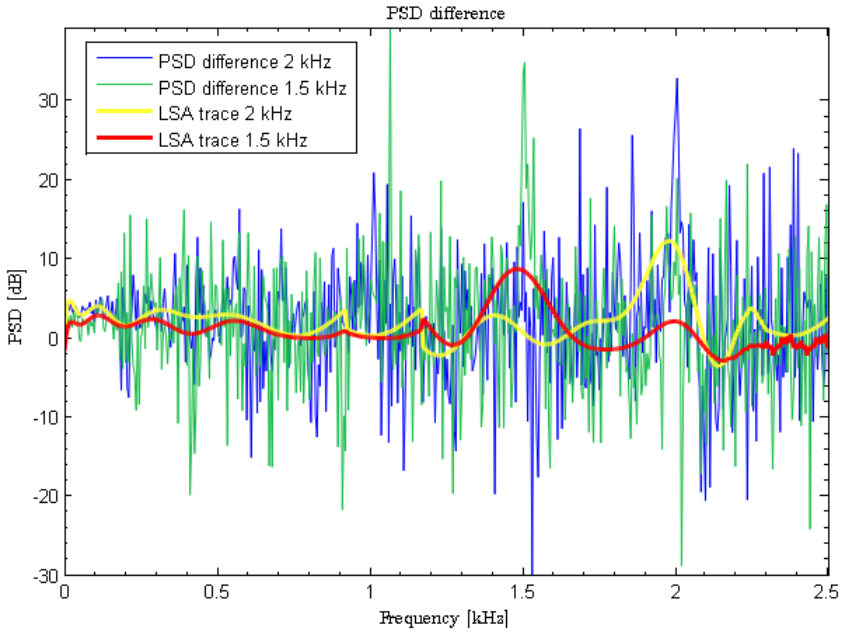

(b) Difference of the two PSDs (with and without acoustic perturbation). The red and yellow lines represent a LSA of the subtractions performed. The two acoustic frequencies peaks are highlighted at 1.5 kHz and 2 kHz.

Figure 4.8: PSD of the second setup.

Also for this setup has been performed the moving average of **M** and after deleting the 1 kHz noise peaks the figure (4.9, 4.10) are obtained. In this case the first coil has been affected by an acoustic wave of 2 kHz while the second coil has been perturbed by an acoustic wave at 1.5 kHz. The two coils have been isolated and inserted in a cartoon box, but as can be seen from the graph, the two coils have not been acoustically separated.

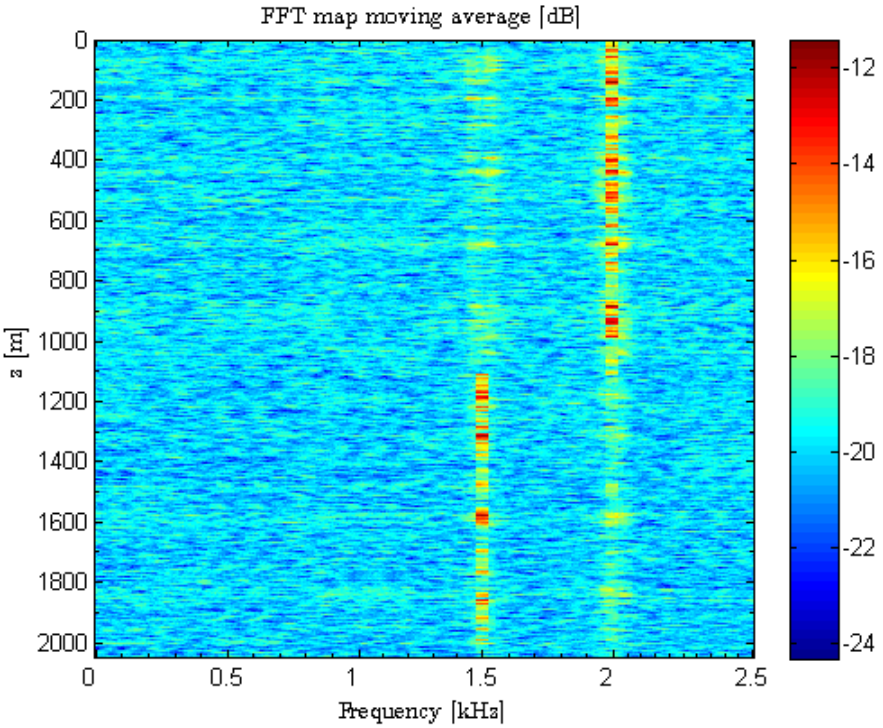

Figure 4.9: Representation of matrix $\mathcal{F}(\mathbf{M})$ in dB units.

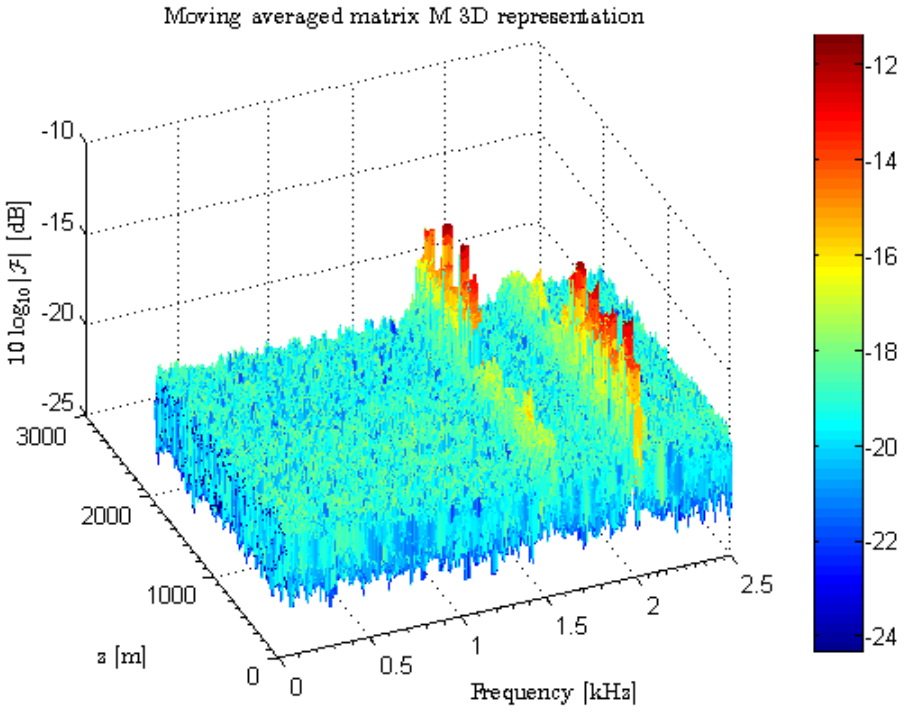

Figure 4.10: Representation of matrix $\mathcal{F}(\mathbf{M})$ as a 3D graph, in dB units.

4.3 Setup 3

This setup has been realized as depicted in figure (3.19). The measured trace is presented in figure (4.11(a)), in which it is possible to identify the events that characterize this setup. In addition to that it is possible to see the length of the used coils which correspond to a total of $\sim 7.21\ km$.
In figure (4.11(b)) has been depicted only the coil 3 measurements, in blue, and, in red, the first order LSA line. In this case the attenuation for coil 2 is $\alpha \sim 0.23\ dB/km$, which is similar to the value read on the coil label.

Also in this setup noise frequencies peaks are presented around the 1 kHz frequencies. The spectrum without the acoustic perturbation is depicted in figure (4.12(a)).

In this setup has been chosen to perturb the two fibre cables that link coil 1 to coil 2, and, coil 2 to coil 3, with the same acoustic wave at 700 Hz. In figure (4.2(b)) is depicted the spectrum of the setup 3 measure, with the two fibre cables affected by a 700 Hz acoustic wave.
Successively has been calculated the PSD, as done for the previous setup, and as expected there is a peak around 700 Hz. In order to make it clearer has been performed the subtraction between PSD, of the measure without acoustic perturbation, and the PSD with the acoustic perturbation; this is depicted in figures (4.13(a),4.13(b)). In figure (4.13(a)) can also be observed the spectral leakage phenomenon.

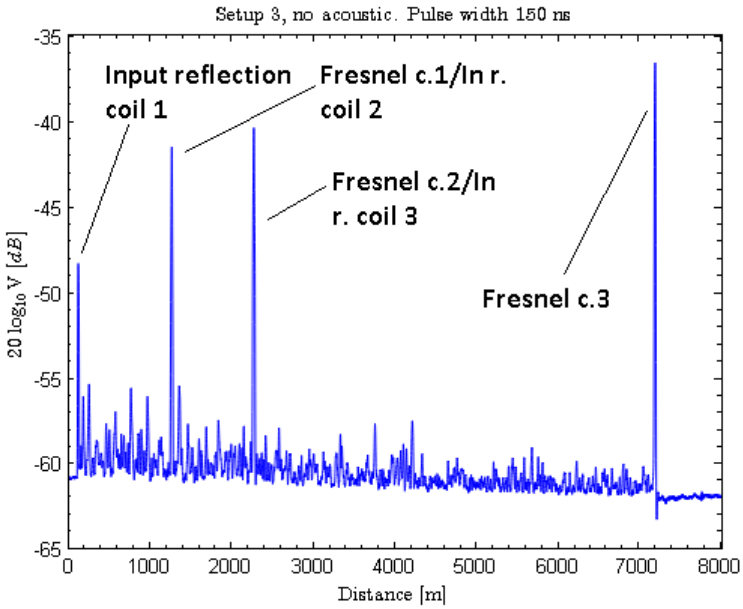

(a) Trace, with identified events, of the third setup.

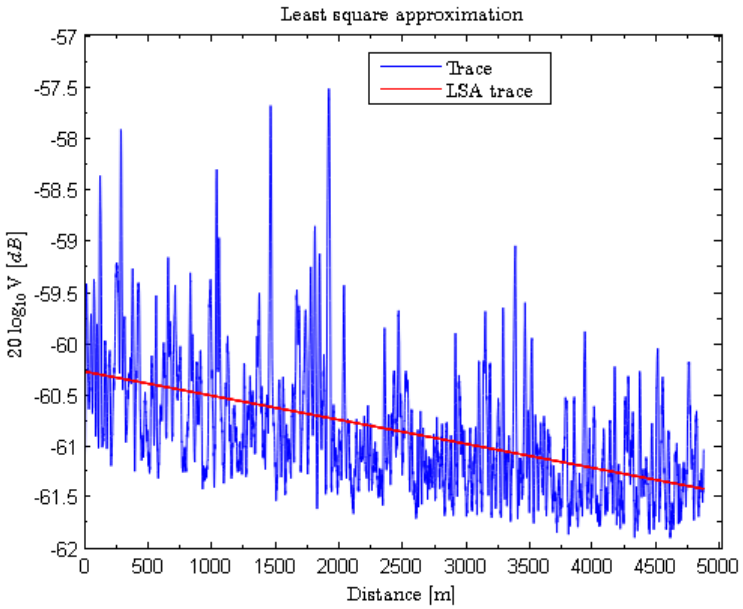

(b) Part of the trace ($\sim 5\ km$) of the third setup (only the *coil 1* samples, except for the input and output peaks) in which has been applied the Least Square Approximation (LSA) method in order to reduce the uncertainty of the measure for the attenuation α.

Figure 4.11: Measured trace of the third setup.

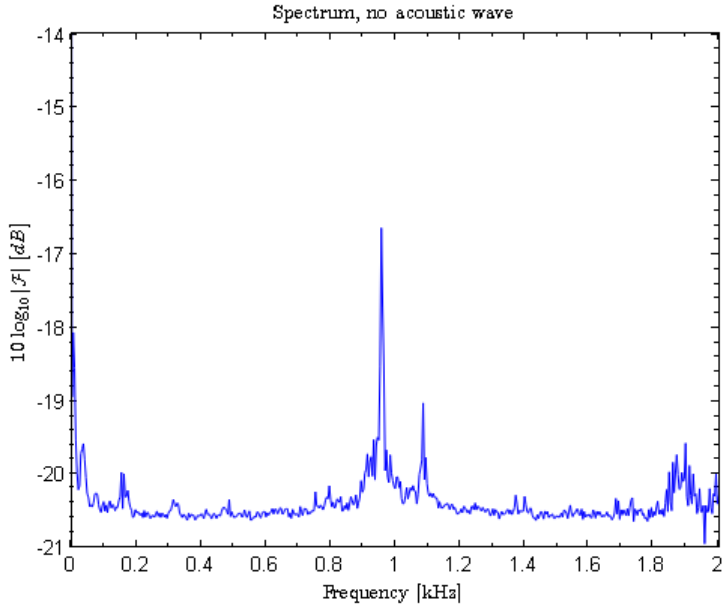

(a) Spectrum of the setup 3 trace, without the acoustic wave perturbation.

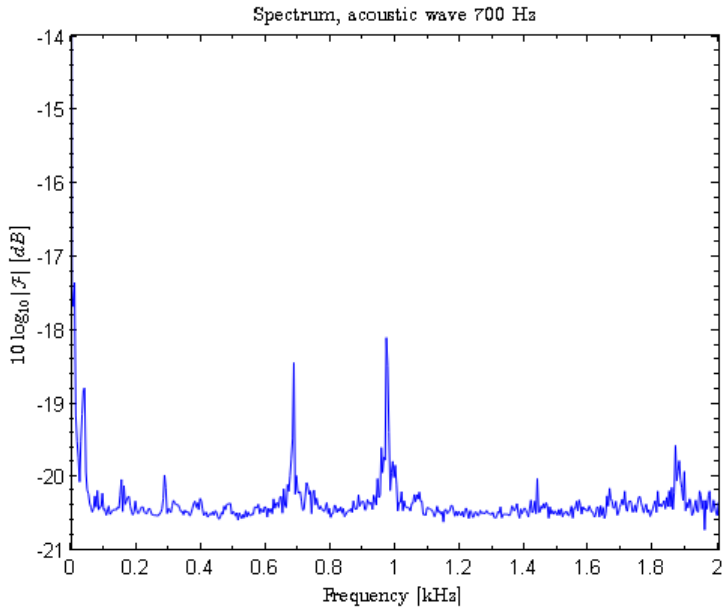

(b) Spectrum of the setup 3 trace, with the acoustic wave perturbation at 700 Hz.

Figure 4.12: Spectrum of the third setup measure.

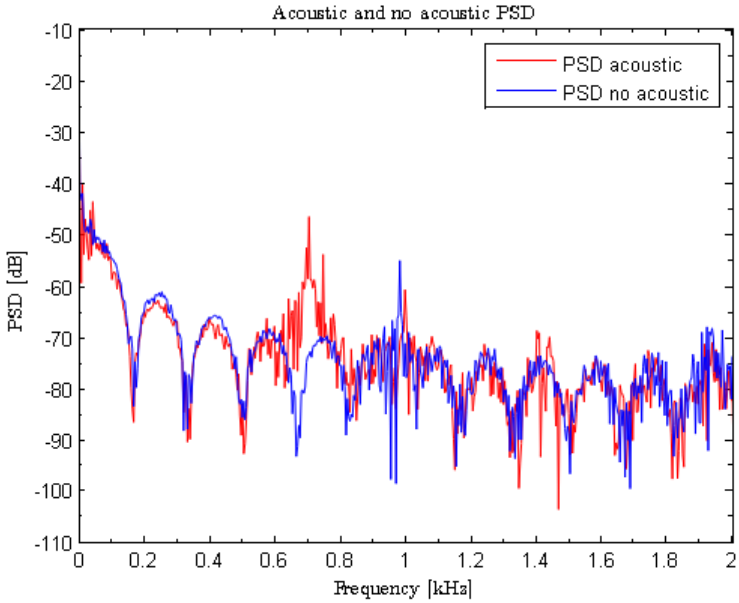

(a) Overlapped PSDs of the two measured traces (with acoustic wave at 700 Hz and without acoustic wave).

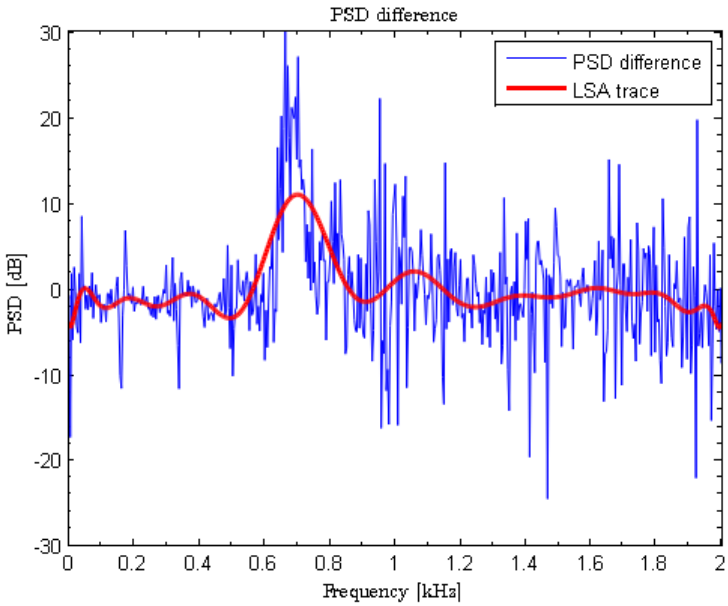

(b) Difference of the two PSDs (with and without acoustic perturbation). The red line represents a LSA curve in order to highlight that the PSD peak is around the given frequency of 700 Hz.

Figure 4.13: PSD of the third setup.

Also for this setup has been performed the moving average of **M** and after deleting the 1 kHz noise peaks the figure (4.14, 4.15) are obtained. In figure (4.14) there are two horizontal lines around 1 km and 2 km which corresponds to the reflections peaks in between the first and the second coil, and in between the second and the third coil. In this graph these peaks couldn't been removed because the acoustic wave perturbation was localized very close to these peaks. In fact in between the two coils has been positioned the fibre ~ 10 m of cable under test. The small spots have been localized as expected, at the frequency of 700 Hz at the correct position. A better comprehension of the acoustic wave perturbation can be done looking at figure (4.15), where at the frequency of 700 Hz the two acoustic perturbation peaks stand out with respect to the others peaks due to EDFAs noise.

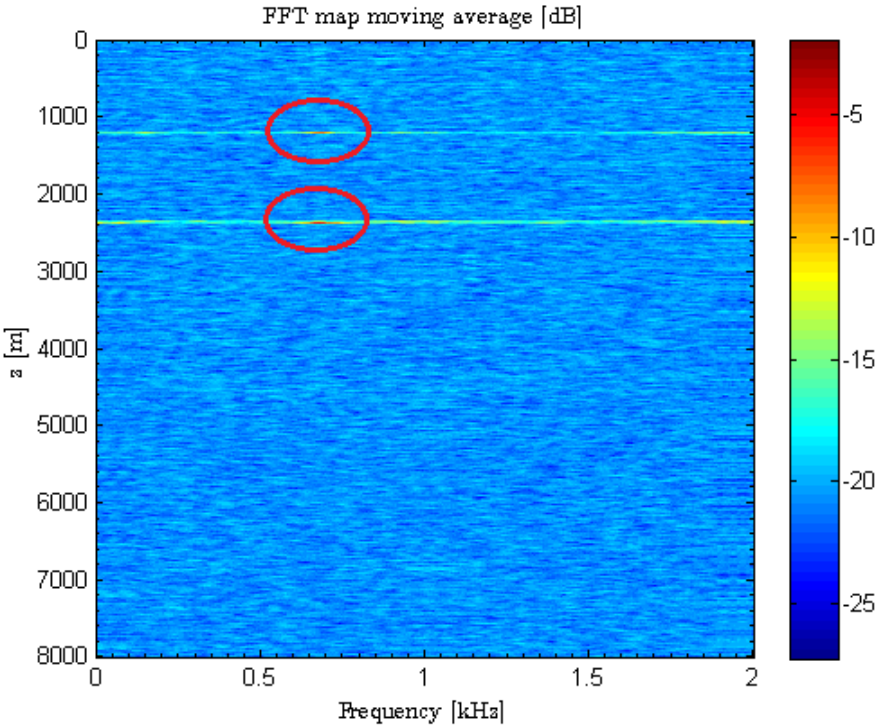

Figure 4.14: Representation of matrix $\mathcal{F}(\mathbf{M})$ in dB units.

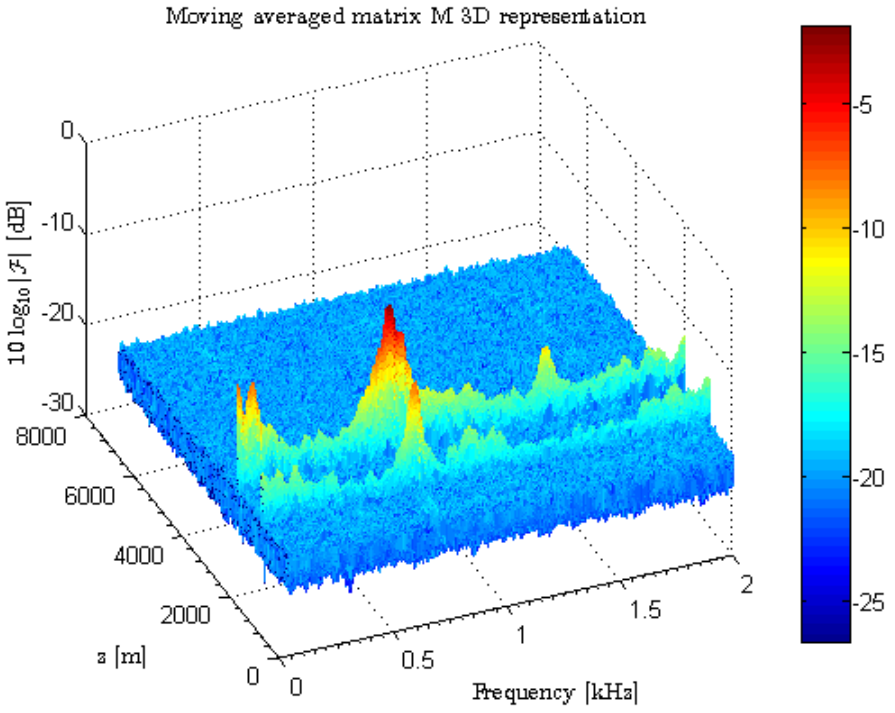

Figure 4.15: epresentation of matrix $\mathcal{F}(\mathbf{M})$ as a 3D graph, in dB units.

5

Conclusions

In this thesis a fibre optic distributed acoustic sensor, exploiting the Φ-OTDR acquisition technique, has been developed. As first step of this work an optimal configuration has been implemented. In fact the first goal was to maximize the input power, at the optical fibre input, and to "minimize" the noise level, with respect to the two options: AOM + EDFA and EDFA + AOM. In this way the setup with the better SNR, at the input of the sensor, and consequently also to the receiver side, has been implemented. Successively the setup 1, with one coil, has been realized. With this configuration has been tested that effectively the system could measure a high number of traces, along the z direction, in order to perform a correct sample of the acoustic wave. The spectrum analysis of that trace showed that the acoustic wave perturbation along all the fibre was effectively captured and displayed in the frequency domain.
A second setup has been realized in order to highlight that this system can discriminate both the acoustic wave frequencies which perturb the two coils and the positions at which these perturbations are localized. Finally a third setup has been implemented with the addition of another coil. In this final setup the objective was to localize the perturbations of the acoustic wave, at a given frequency, and to highlight the fact that this is a *distributed* sensor, and for this reason it is

possible to localize events which come up in small sections of the system.
This setup can be widely improved both increasing the power transmitted into the optical fibre and substantially increasing the number of acquisitions per measurement session. In this way it will be possible to discriminate in a better way the *acoustic dots* in the spectrum map and also to detect different kinds of acoustic perturbations which can be also subjected to variations along a time interval of seconds. Increasing the measured time is then possible to obtain a real-time system monitoring.
Other improvements can be made on the setup, using as receiver part an interferometer structure based on 3x3 coupler for increasing the sensitivity, decreasing the noise and directly obtaining phase, amplitude, frequency response and location information without performing the FFT.

Bibliography

[1] A. Masoudi, M. Belal, and T. P. Newson. *A distributed optical fibre dynamic strain sensor based on phase-OTDR.* Meas. Sci. Technol., vol. 24, no. 8, p. 085204, Jul. 2013. URL: http://eprints.soton.ac.uk/356341/.

[2] Agilent Technologies. *Optical Time Domain Reflectometers.* 2001. URL: http://literature.cdn.keysight.com/litweb/pdf/E6000-91017.pdf?id=65325.

[3] Bahaa E. A. Saleh, Malvin Carl Teich. *Fundamentals of Photonics, 2nd Edition.* April 2007.

[4] Boyd RW. *Nonlinear optics.* Nonlinear optics. 3rd ed New York: Academic Press 2008.

[5] Corning. *Basic Principles of Fiber Optics*. 2005. URL: www.corningcablesystems.com/web/college%20/Fibretutorial.nsf/ofpara.

[6] J. C. Palais. *Fiber Optic Communications*. Upper Saddle River, NJ: Prentice Hall, 1998. URL: http://adsabs.harvard.edu/abs/1998foc..book.....P.

[7] JC Juarez. *Distributed fibre optic intrusion sensor system for monitoring long perimeters*. 2005. URL: https://oaktrust.library.tamu.edu/bitstream/handle/1969.1/ETD-TAMU-1702/JUAREZ-DISSERTATION.pdf?sequence=1&isAllowed=y.

[8] Jeremiah Francis Kimbell. *History and analysis of distributed acoustic sensing (DAS) for oilfield applications*. August 2013. URL: http://oaktrust.library.tamu.edu/bitstream/handle/1969.1/150995/KIMBELL-THESIS-2013.pdf?sequence=1.

[9] Luca Palmieri, Luca Schenato. *Distributed Optical Fiber Sensing Based on Rayleigh Scattering*. 2013. URL: http://benthamopen.com/contents/pdf/TOOPTSJ/TOOPTSJ-7-104.pdf.

[10] National Telecommunications and Information Administration. URL: http://www.its.bldrdoc.gov/fs-1037/dir-001/_0133.htm.

[11] P. Healy. *Review of long wavelength single-mode optical fibre reflectometry techniques*. pp. 876–886, Aug. 1985. URL: http://cat.inist.fr/?aModele=afficheN&cpsidt=8566114.

[12] Q. He, T. Zhu, X. Xiao, B. Zhang, D. Diao, and X. Bao. *All fibre distributed vibration sensing using modulated time-difference pulses*. Photon.

Technol. Lett., vol. 25, no. 20, pp. 1955−1957, Oct. 15, 2013. URL: http://ieeexplore.ieee.org/stamp/stamp.jsp?arnumber=6582659.

[13] R. Sifta, P. Munster, P. Sysel, T. Horvath, V. Novotny, O. Krajsa, M. Filka. *Distributed fiber-optic sensor for detection and localization of acoustic vibrations*. Metrol Meas Syst, 22 (1) (2015), pp. 111−118.

[14] Roberto Limina. *Distributed Optical FIber Sensing*. 2010. URL: http://tesi.cab.unipd.it/25942/1/Tesina_Roberto_Limina_493851_TC.pdf.

[15] Signatec, Incorporated. *PDA14 Operator's Manual*. October 2005.

[16] Yahei Koyamada, Mutsumi Imahama, Kenya Kubota, and Kazuo Hogari. *Fibre-Optic Distributed Strain and Temperature Sensing With Very High Measurand Resolution Over Long Range Using Coherent OTDR*. 2009. URL: http://ieeexplore.ieee.org/stamp/stamp.jsp?tp=&arnumber=4840627.